ELSEVIER

Carbohydrate Research 298 (1997) 15–49

CARBOHYDRATE RESEARCH

A comparison of the geometry and of the energy results obtained by application of different molecular mechanics force fields to methyl α-lactoside and the C-analogue of lactose

Manuel Martín-Pastor, Juan Félix Espinosa, Juan Luis Asensio, Jesús Jiménez-Barbero *

Grupo de Carbohidratos, Departamento de Química Orgánica Biológica, Instituto de Química Orgánica, C.S.I.C., Juan de la Cierva, 3, 28006 Madrid, Spain

Received 1 July 1996; accepted 8 September 1996

Abstract

The applicability of a number of standard molecular mechanics force fields, namely AMBER/Homans, CVFF, CFF91, ESFF, and MM3*, and of the AM1 semiempirical Hamiltonian, to the molecular modelling of methyl α-lactoside is described. A protocol based on the calculation of relaxed energy maps for a significant number of initial structures has been employed. Different dielectric constants, as well as a continuum model solvent have been used. The geometric characteristics (distances and torsion and valence angles) of the low energy minima have been gathered and compared to experimental solution NMR and solid state X-ray data. Concerning the energies, the relative steric energy values provided by the different programs have been translated into ensemble average distributions of conformers which, in turn, have been employed to generate NMR parameters, i.e. NOE, NOESY, and ROESY intensities and homo- and hetero-nuclear coupling constants. The results indicate that MM3* and CVFF provide conformer distributions which account for the solution NMR observables in a satisfactory way. AMBER/Homans provide a reasonable agreement, while conformational analysis of oligosaccharides by AM1, ESFF, and CFF91 is not advised. The best fit between the experimental X-ray distances and angles and the modeling studies is found when CVFF is used. Results from the different force fields (and AM1) for C-lactose were compared.

Keywords: Methyl α-lactoside; Molecular mechanics; NMR; NOESY; ROESY; Coupling constants

* Corresponding author.

0008-6215/97/$17.00
PII S0008-6215(96)00225-X

1. Introduction

A prerequisite to the full understanding of the biological function of carbohydrates is access to detailed descriptions of their three dimensional structures [1]. Unfortunately, crystallographic data on medium-sized and large oligosaccharides are rather limited [2]. In addition, the experimental evidence indicates that many oligosaccharides are potentially flexible molecules [3]. Therefore, the elucidation of the conformation of carbohydrates in solution is usually performed by a combination of NMR spectroscopy and molecular modelling techniques [4]. Nevertheless, there are still important problems with oligosaccharide force field calculations, which mainly arise from the lack of generally valid parameter sets [5]. As a result, different general purpose molecular mechanics force fields have been used with [6] or without [7] modifications to perform conformational analysis of carbohydrates. The major modifications usually concern the inclusion of explicit energy terms to deal with the anomeric effects [8,9]. We have previously reported [10] the use of different potential energy functions, namely, AMBER as modified by Homans, CVFF, and CFF91 in order to test the use of these force fields in conformational studies of carbohydrates [11]. We chose methyl β-galactopyranosyl-(1 → 4)-α-glucopyranose (methyl α-lactoside, **1**, Fig. 1) as a model compound, since a great deal of experimental NMR [10] and X-ray parameters [12] are available for this molecule. We now extend the comparison by considering two additional force fields, namely MM3* and ESFF, and we also include in the analysis the results obtained by application of the semiempirical molecular orbital AM1 Hamiltonian. To evaluate the relative steric energies provided by the different methods, for every force field (and AM1), the calculated ensemble average distributions of conformers [13] have been used to predict the intensities of nuclear Overhauser enhancements [14], measured under different experimental conditions, as well as homo- and hetero-nuclear coupling constants [15]. In addition, calculated geometric parameters including interatomic distances, and valence and torsion angles have also been compared to the previously reported X-ray structure of α-lactose [12]. The possible variability of the shape of the gluco- and galacto-pyranoid rings may heavily influence both intra- and inter-residue distances which, in turn, affect the calculated NOE and relaxation parameters. Besides, the shapes of higher oligomers built from the monosaccharide or disaccharide geometries may differ dramatically depending on the force field used to generate the starting building block [16]. Similar calculations, by using the five force fields, have also been performed for the C-glycoside analogue of compound 1, (C-lactose, **2**) for which NMR parameters have been measured recently [17].

2. Experimental

Conformational calculations. Molecular mechanics.—Glycosidic torsion angles are defined as ϕ H-1′–C-1′–O-1′(C-α)–C-4 and ψ C-1′–O-1′(C-α)–C-4–H-4 for **1**(**2**). Relaxed (ϕ,ψ) potential energy maps were calculated for **1** using AMBER/Homans [18], CVFF [19], CFF91 [20], MM3* [21] and ESFF [22]. MM3* was employed as integrated in MACROMODEL 4.5 [23]. AMBER/Homans, CVFF,

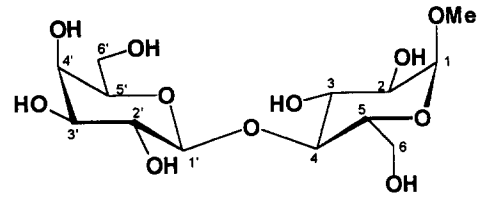

1

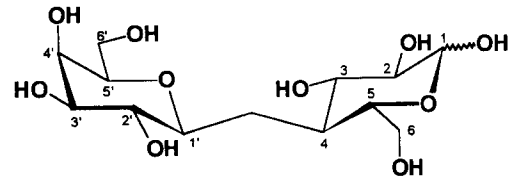

2

Fig. 1. View of methyl α-lactoside (**1**) and C-lactose (**2**) along with the atomic numbering.

CFF91, and ESFF were used as integrated in DISCOVER (Biosym technologies). Only the gg and gt orientations of the primary alcohol group were used for the glucose moiety, while tg and gt conformations were used for the galactose residue, since they have been shown to be rather more stable than the alternative tg or gg conformers, respectively [24]. Thus, four combinations were taken into account, namely, gggt, gtgt, ggtg and gttg. The first two characters correspond to the glucose unit, and the other two, to the galactose one. The starting positions for the secondary hydroxyl groups were r (anti-clockwise) or c (clockwise) giving four stable combinations: rr, rc, cr or cc (clockwise). The first character corresponds to the glucose ring while the second belongs to the galactose. Therefore, sixteen initial geometries were considered and sixteen different relaxed energy maps were built. Different dielectric constants were employed, at least two: $\varepsilon = 1$ and $\varepsilon = 80$. In addition, the GB/SA solvent model [25] for water ($\varepsilon = 1$) was also used in the MM3* calculations. A total of 6400 conformers (14,400 for AMBER/Homans) were calculated for each case. The previous step involved the generation of the corresponding rigid residue maps by using a grid step of 18° (12° for AMBER/Homans). Then, every (ϕ,ψ) point was minimized by 2500 conjugate gradient iterations. Following this protocol, the rms derivatives in low energy regions were smaller than 0.05. Despite the constraint set for the torsion angles of the glycosidic linkage (15,000 kJ/rad^2), deviations nearly as large as 3° in ϕ/ψ values were observed in high energy regions. From these relaxed energy maps, adiabatic surfaces were built by choosing the lowest energy for a given ϕ,ψ point. Therefore on these surfaces, which represent a two-dimensional projection of a multidimensional hyperspace, points coexist which come from different geometries in terms of the secondary hydroxyls and hydroxymethyls. The comparison for C-lactose (**2**) was less detailed. Sixteen relaxed energy maps were computed with the MM3* force field and $\varepsilon = 80$. In the other cases, only the major conformers included in the three predominant regions of the computed map for the corresponding O-glycoside [10,11] were minimized, with every field/dielectric constant.

Computational methods.—The MM3* force field [21] is highly detailed and includes the anisotropy of hydrogens; corrections for stereoelectronic effects; cross-term effects like torsion stretch, torsion bend, and bend–bend interactions; a Buckingham-type potential for non-bonded interactions; and an explicit term for hydrogen bonding. MM3* differs from the regular MM3 force field in the treatment of the electrostatic terms, since it employs charge–charge instead of dipole–dipole interactions. The possibility of employing the GB/SA solvation [25] model in conjunction with MM3* makes its use particularly attractive for oligosaccharide solution studies.

CFF91 is also a Class II force field [20]. It uses the Morse potential to model covalent bonds and includes an anomeric carbon atom. It has been developed by the use of the consistent force field approach using least square fitting on experimental data like internal coordinates, non-bonded distances, dipole moments, lattice energies, unit cell dimensions, and vibrational frequencies. Both anharmonic diagonal terms and cross terms are included in the potential energy function. Environmental variables have been explicitly taken into account, but energetic data of rotameric isomers have not been included. This force field does not posses an explicit hydrogen bonding potential. Van der Waals interactions are represented by a 6–9 power term.

The AMBER force field has been used widely for proteins and DNA and its use has been extended to carbohydrate molecules [18]. This force field is fairly simple and employs an harmonic potential to treat the bond-stretching, and two more terms for angles and torsions. It also includes a van der Waals term, an electrostatic term and a simple term for the hydrogen bonding interaction by increasing the electrostatic description of the hydrogen bond. Explicit hydrogens have been used in the present study.

CVFF [19] is a generalized valence force field, which was originally created to reproduce peptide and protein properties. It has been extended to handle more general systems. It uses a Morse potential for the bond-stretching term and presents a number of cross terms. Hydrogen bonds are a natural consequence of the standard van der Waals and electrostatic parameters.

ESFF (extensible systematic force field) [22] is a new rule-based force field, which is still under development. It relies on atomic parameters coupled with rules for generating explicit parameters. As much as possible, the atomic parameters are directly determined from experiment or calculated rather than fit. Only diagonal terms are included. Van der Waals interactions are represented by an 6–9 potential and the corresponding parameters are affected by the charges of the atoms.

Semiempirical calculations: AM1.—The AM1 Hamiltonian [26] is a reparameterized version of MNDO [27] with changes in the core–core repulsion

function designed to eliminate the spurious repulsions. In principle, AM1 is able to reproduce hydrogen bonding and the distortion of bond lengths associated with the anomeric effects.

Due to the large amount of time necessary for quantum mechanical calculations, only two relaxed (ϕ,ψ) potential energy maps (in fact, heats of formation) were calculated for **1** at the AM1 level. Both gg and gt rotamers of the hydroxymethyl group of the glucose moiety were used, while the experimentally most abundant gt rotamer of the galactose unit was employed [10,11]. The cr combination of the secondary hydroxyl groups was used, since it was always the most stable for all the molecular mechanics studies reported to date [28]. A total of 648 conformers were calculated. The previous step involved the generation of the corresponding rigid residue maps by using a grid step of 20°. Then, every (ϕ,ψ) point was minimized, by using the AM1 semiempirical method as integrated in MOPAC, V 6.0, and the BFGS procedure. Following this protocol, the gradient norm of the minimized structures was smaller than 0.042 kJ mol^{-1}Å^{-1}. The PRECISE option was used to ensure an adequate convergence criterion. The three lowest energy local minima obtained were fully optimized and their geometries subsequently characterized.

The solvation energies of the three minima obtained by AM1 were estimated using the semiempirical solvent model SM2 [29] as implemented in the AMSOL package. The geometry remained basically unaltered, although changes in the relative energy values of the minima were observed.

Probability calculations.—From the relaxed energy maps, calculated for each dielectric constant, the probability distribution [13] was calculated for each ϕ/ψ point. Assuming that the entropy difference among the different conformers is negligible, the probability P for a given ϕ/ψ point is:

$$P_{\phi/\psi} = \Sigma_i\{\exp(-\Sigma_i/RT)\} / \Sigma_i\Sigma_{\phi\psi}\{\exp(-\Sigma_{i\phi\psi}/RT)\}$$

This relationship can be used in a simple way to transform energy maps into probability maps. In our case, the sum of the numerator extends over the number of relaxed energy maps. The sum of the denominator considers the number of calculated points.

The single point calculations [5] were performed by using the same formula, but only taking into account the local minima of the adiabatic map.

NOE calculations.—The first step in the NOE calculation was to estimate the interproton average distances according to $\langle r^{-3}\rangle_{kl}$ and $\langle r^{-6}\rangle_{kl}$ averages.

The estimated probability distributions were used to calculate the average distances, assuming a Boltzmann distribution of conformers:

$$\langle r^{-6}\rangle_{kl} = \Sigma P(\phi\psi)^{*} r_{kl}^{-6}(\phi\psi)$$

The steady state NOEs, NOESY, and ROESY spectra, and non-selective T_1s were simulated according to the complete relaxation matrix method, assuming isotropic motion [10], a correlation time of 0.06 ns, and external relaxation of 0.1 s^{-1} in different calculations. All the spectra were simulated from the average distances $\langle r^{-6}\rangle_{kl}$ calculated from the relaxed energy maps at 300 K. In the case of the steady NOEs, the calculations were performed by solving the simultaneous set of linear equations proposed by Noggle and Schirmer [30], while the NOESY and ROESY spectra were simulated according to the protocol outlined by Cagas and Bush [31], using different mixing times. All the NOE calculations were automatically performed by a local program which is available from the authors upon request.

3. Results and discussion

Methyl α-lactoside.—Molecular mechanics and semiempirical calculations. Fig. 1 shows the structure of methyl-α-lactoside along with the atomic numbering. The analysis of the molecular mechanics calculations performed for **1** using AMBER/Homans, CVFF, and CFF91 has been reported already [10,11] and, therefore, these results will be only summarized here.

MM3 calculations.* Sixteen relaxed energy maps were calculated for methyl-α-lactoside by MM3*, using $\varepsilon = 1$, 80, and the GB/SA solvation model [11]. The shapes of the surfaces depend on the initial orientation of the secondary hydroxyl groups, and although less pronounced, also on the hydroxymethyl groups. Table 1 shows the probability distribution for the different dielectric constants. For $\varepsilon = 1$, about 98% of the population can be located around the cr disposition while the hydroxymethyl groups have mostly gggt and gtgt conformations. MM3* at this low dielectric constant predicts a 70:30 ratio between the gg:gt rotamers of the Glc unit and a 91:9 equilibrium between the gt:tg rotamers of the Gal moiety. The adiabatic map, calculated for $\varepsilon = 1$, is shown in

Table 1
Steric energy values and populations of the low energy regions of compound **1** estimated from different force fields

	CVFF				CFF91				ESFF			
Conf.	A	C	B	D	A	C	B	D	A	C	B	D
ϕ/ψ	23/176	166/4	48/0	−29/−27	17/179	170/−2	47/−11	−13/−30	36/180	162/0	54/0	−32/−33
ΔE, $\varepsilon = 1$ (kJ/mol)	10.1	5.1	0.0	6.2	19.0	13.4	11.6	0.0	8.8	0.0	10.4	9.2
Ave. pop. (%)	1	3	96		< 1	> 1	98		2	95	3	
ΔE, $\varepsilon = 80$ (kJ/mol)	12.8	8.1	0.0	–	8.4	7.0	1.3	0.0	1.3	5.0	0.0	2.9
Ave. pop. (%)	< 1	> 1	98		2	1	97		20	1	79	
	AMBER			MM3*			AM1					
Conf.	A	B	C	A	B	C	A	B	C			
ϕ/ψ	60/−156	48/0	168/0	36/180	54/2	180/−18	63/−150	49/1	170/−4			
ΔE, $\varepsilon = 1$ or 1* r (kJ/mol)	23.7	11.3	0.0	15.8	0.0	15.3	0.0	2.58	8.12			
Ave. pop. (%)	0	< 1	> 99	< 1	> 99	< 1	44.0	50.5	5.5			
ΔE, $\varepsilon = 80$ (kJ/mol)	1.3	0.0	1.1	8.5	0.0	23.2						
Ave. pop. (%)	15	70	15	2	98	< 1						
ΔE, H_2O (kJ/mol)				18.0	0.0	14.1						
Ave. pop. (%)				< 1	> 99	< 1						

Fig. 2 and shows a broad low energy region, centered around minimum B (*syn*) with ϕ/ψ values of 54.0°/−16.4°. This minimum shows a hydrogen bond, HO-3 · · · O-5′, that of crystalline lactose [12]. There are also two regions of higher energy, minima C and A centered around ϕ/ψ values of −179.9°/−17.7° and 36.0°/−179.0° (conformer *anti*), respectively. Conformer C shows two hydrogen bonds, O-2′ · · · HO-3 and HO-6′ · · · O-6. All these minima are in agreement with the operation of the exo-anomeric effect and are shown in Fig. 3. The corresponding population distribution map (Fig. 2) shows that the region represented by minimum B is highly populated, with a single point population of

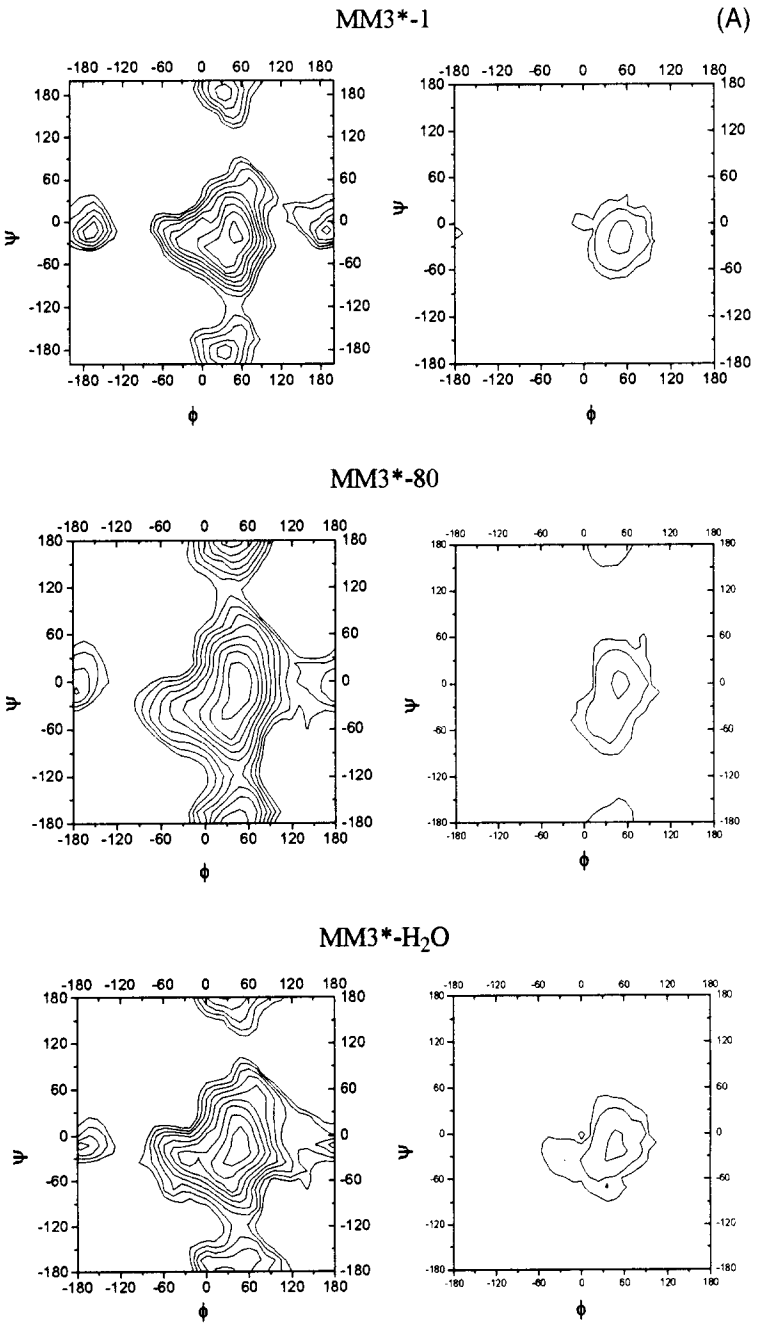

Fig. 2. (A) Steric energy (left) and probability maps (right) determined by MM3* for methyl α-lactoside using different dielectric conditions. The energy levels are represented every 4.18 kJ/mol and the probability levels at 10%, 1% and 0.1%. (B) Steric energy (left) and probability maps (right) determined by ESFF for methyl α-lactoside using different dielectric conditions. The energy levels are represented every 4.18 kJ/mol and the probability levels at 10%, 1%, and 0.1%.

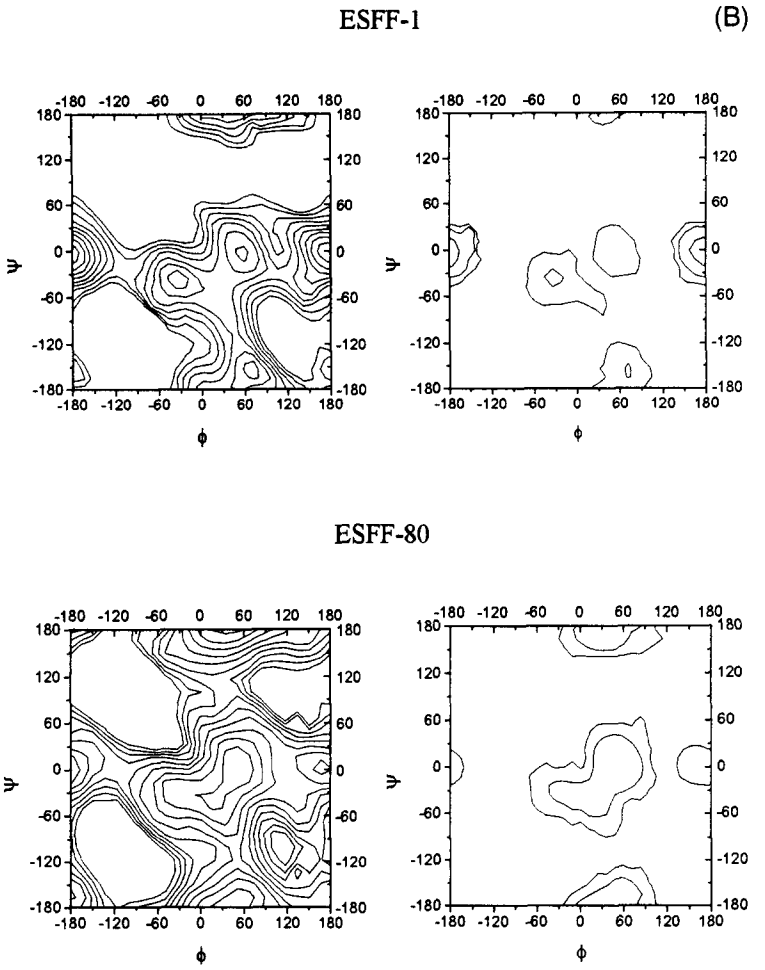

Fig. 2 (continued).

99.6%, while those corresponding to minima A and C are scarcely populated with 0.2% each (Tables 2 and 3). The energy barriers between the regions are rather high: that between minima C and B is about 41.8 kJ/mol, while that between B and A is approximately 33.4 kJ/mol.

The surfaces obtained for **1** by using $\varepsilon = 80$ showed that the sensitivity of the surface to the initial structure was much smaller than for $\varepsilon = 1$. The probability distribution of these maps was also different from the one obtained for $\varepsilon = 1$. Hence the most populated conformations of the hydroxyls are cr and rr (68% and 26%, respectively) while the hydroxymethyl groups mostly adopt the gtgt and gggt orientations (61% and 34%, respectively). In fact, the ratio of rotamers for the Glc and Gal hydroxymethyl groups is gg:gt, 36:64, and gt:tg, 95:5, respectively (Table 4). The corresponding adiabatic map is shown in Fig. 2. The low energy region, around minimum B with ϕ/ψ values of 54.0°/1.4°, and the other two local minima areas are similar to those described above for $\varepsilon = 1$. The area around minimum B has now a single point population of 96.6%, while the rest of the population is contained around conformer A (*anti*). This region contains all known structures of lactose structures. Nevertheless, the possibility of the existence of conformers A and C in solution can not be discarded since they have been detected for some β-(1 → 4) linked interglycosidic synthetic acetals of lactose and cellobiose [32] and for an oligosaccharide bound to a lectin [33]. The energy barriers between the regions are now smaller than at low dielectric constant: that between minima C and B is about 33.4 kJ/mol, while that between A and B is only 20.9 kJ/mol.

The 16 potential energy surfaces obtained by using the GB/SA solvent model [25] for water again present a high sensitivity to the initial structure, as observed when using $\varepsilon = 1$. The probability distribution deduced from these maps shows again that the cr

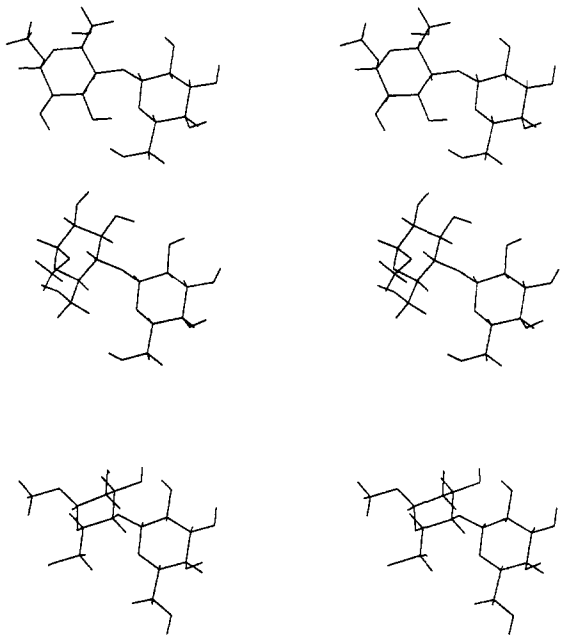

Fig. 3. Stereo view of the major minima of methyl α-lactoside calculated by MM3*. The interglycosidic torsion angles are fairly similar to those obtained by the different force fields. From top to bottom, conformers A, B, and C (see text).

geometry is the most populated one (97%), while the hydroxymethyl groups basically adopt the gggt and ggtg (69% and 21%, respectively) orientations. The rotameric distribution is now gg:gt, 90:10, for Glc, and gt:tg, 77:23 for Gal. The adiabatic map is shown in Fig. 2. The population distribution is fairly similar to that described for $\varepsilon = 1$, with a major conformer (B) with a population of 99.9. The corresponding energy surface is now quite smooth: the barrier between minima C and B is about 29.3 kJ/mol, while that between B and C is only 12.5 kJ/mol.

Dowd at al. have calculated the potential energy maps for both cellobiose anomers [34] (also with a β-(1 → 4) glycosidic linkage), using the regular MM3 force field, and using $\varepsilon = 4$. Although lactose and cellobiose differ in the configuration at C-4 of the Gal moiety, it can be observed that the global characteristics of their maps are fairly similar to those deduced herein with the MM3* force field and $\varepsilon = 80$. In particular the rr and cr orientations of the secondary hydroxyls occur more frequently in both cases. With regard to the orientation of the hydroxymethyl group of the Glc moiety, the gt rotamer is also favoured in both examples (here with $\varepsilon = 80$). Nevertheless, the best agreement with the experimental results is found herein with $\varepsilon = 1$ (see below under comparison to NMR data). With regard to the torsion angle values of the corresponding minima differences smaller than 5° in ϕ and than 20° in ψ are found. Very recently, force field calculations, also with the regular MM3 program [35], have been performed for ethyl β-lactoside and $\varepsilon = 4$. In this case, the three major A, B, and C conformers were also found, with similar geometries around the glycosidic linkages. At this dielectric constant, both gt rotamers of the hydroxymethyl groups are favoured, as described here for $\varepsilon = 80$.

ESFF calculations. With this force field and $\varepsilon = 1$, the form of the low energy regions is extremely dependent on the initial orientation of the secondary hydroxyls and of the hydroxymethyl groups [11]. The adiabatic surface is shown in Fig. 2B. There are four local minima below a steric energy level of 16.7 kJ/mol (Tables 1 and 2). For this force field and dielectric constant, the central region of the map, clearly splits into two well separated areas, one for positive ϕ (minimum B) and one for negative ϕ (minimum D). Minimum D is separated from the favoured exo-anomeric position. Although this area does not show any intraresidue hydrogen bond, a geometry similar to this conformation has been recently proposed as the bound conformation of methyl α-lactoside to ricin-B lectin in solution [36]. According to the probability distribution, 85% of the population is located in region C, 9% around B/D, and 6% is around minimum A. The energy barriers between the minima are smaller than 20.9 kJ/mol. As will be shown below, there is null concordance with the experimental results both in solution [10] and in the solid state [12] (for **1** and different analogues). The position of the secondary hydroxyl groups is rather important for the final results observed in the analysis, since for the cr orientation, 90% of the population is located around conformer *syn*-B, in the central region of the map. This is not the case for the cc, rc, and rr orientations. In the cr orientation, there is no possibility of formation of the strongly stabilizing HO-2′–O-3 hydrogen bond of minimum C, since, for cr, the corresponding atoms do not have as adequate orientation, and, in addition, both hydrogen atoms come into close contact, destabilizing conformer C. The global probability distribution is shown in Table 1, and the rr configuration appears populated to more than 92% extent. The Glc gt conformer dominates the probability distribution, while the conformational equilibrium for the Gal lateral chain is described by a 29:71 distribution for the gt:tg rotamers (Table 4).

When using $\varepsilon = 80$, the sensitivity of the surface to the initial geometry of the hydroxyl/hydroxy-

methyl groups is much smaller than for $\varepsilon = 1$. The adiabatic map is shown in Fig. 2B and the relative energies and populations gathered in Tables 2 and 3. The energy barriers are now smaller than 10.45 kJ/mol. The central *syn* region (minima B/D) dominates the probability distribution (about 77%). Minima A (anti) and C are also significantly populated (3% and 20%, respectively). The associated probabilities for the different orientations of the hydroxymethyl groups are collected in Table 4. There is no

Table 2
Interproton distances for the low energy minima of **1** calculated for the different force fields. The table also contains the distances from the X-ray structure of α-lactose (assuming a C–H bond distance of 1.113 Å)

Force field	Min	H-1′–H-2′	H-1′–H-3′	H-1′–H-5′	H-1′–H-4	H-1′-H-3	ϕ	ψ	ΔE (kJ/mol)	Single point pop.
AMBER-80	A	3.054	2.556	2.309	3.603	2.214	60.0	−156.0	1.3	26.7
	B	3.067	2.578	2.323	2.340	4.513	48.0	0.0	0.0	44.8
	C	3.062	2.563	2.348	3.603	4.571	168.0	0.0	1.1	28.5
AMBER-1* r	A	3.042	2.487	2.378	3.505	2.411	61.2	−144.2	23.7	0.0
	B	3.051	2.490	2.407	2.366	4.523	53.3	−5.5	11.3	1.0
	C	3.047	2.408	2.493	3.579	4.603	169.9	0.2	0.0	99.0
CFF91-80	A	3.069	2.590	2.365	3.611	2.191	17.0	178.6	9.3	2.2
	B	3.074	2.619	2.389	2.396	4.553	45.4	5.7	0.0	94.5
	C	3.077	2.584	2.400	3.630	4.454	169.9	−1.6	8.4	3.3
CVFF-80	A	3.089	2.647	2.460	3.677	2.207	23.1	175.7	12.6	0.6
	B	3.091	2.660	2.480	2.383	4.540	48.2	0.4	0.0	95.5
	C	3.087	2.633	2.465	3.625	4.542	165.8	3.5	8.0	3.9
ESFF-1	A	3.060	2.642	2.546	3.624	2.404	72.0	−161.9	8.5	3.1
	B	3.070	2.593	2.542	2.380	4.516	54.0	0.0	7.7	4.2
	C	3.061	2.570	2.552	3.590	4.420	180.0	0.0	0.0	92.7
ESFF-80	A	3.068	2.651	2.359	3.637	2.093	36.1	180.0	2.0	28.9
	B	3.071	2.652	2.386	2.378	4.542	54.0	0.0	0.0	64.1
	C	3.075	2.662	2.380	3.561	4.551	162.0	0.0	5.5	7.0
MM3*-1	A	3.115	2.580	2.443	3.677	1.994	36.0	−179	15.7	0.2
	B	3.118	2.603	2.388	2.279	4.446	54.0	−16.4	0.0	99.6
	C	3.115	2.453	2.463	3.601	4.471	−179.9	−17.76	15.4	0.2
MM3*-80	A	3.114	2.634	2.384	3.696	1.996	36.0	−179	8.5	3.2
	B	3.113	2.642	2.400	2.372	4.522	54.0	1.5	0.0	96.8
	C	3.109	2.620	2.389	3.645	4.426	−180.0	−17.9	23.2	0.0
MM3*-H_2O	A	3.105	2.597	2.398	3.643	1.996	18.0	−179.2	18.0	0.1
	B	3.117	2.611	2.393	2.299	4.448	54.0	−16.5	0.0	99.6
	C	3.120	2.527	2.370	3.611	4.451	178.6	−3.9	14.1	0.3
AM1	A	3.147	2.676	2.523	3.526	2.326	63.1	−150.1	0.0	71.7
	B	3.149	2.667	2.560	2.308	4.533	48.9	0.7	2.6	25.5
	C	3.151	2.627	2.556	3.579	4.443	166.9	−4.1	8.1	2.8
AM1-SM2	A	3.147	2.675	2.523	3.527	2.329	63.2	−150.1	0.0	85.4
	B	3.149	2.667	2.560	2.307	4.534	48.9	0.8	4.4	14.5
	C	3.151	2.627	2.557	3.579	4.443	166.9	−4.1	16.1	0.1
X-ray lactose	B	3.090	2.680	2.410	2.070	4.110	28.6	−24.3		

predominant orientation of the hydroxyl groups, while for the lateral chains, the predicted distributions are 83:17 (gg:gt) for the Glc unit and 39:61 (gt:tg), for the Gal moiety.

AM1 calculations. The two relaxed energy maps calculated for **1** using AM1 (Fig. 4) are very similar, and generally, as commented above, three low energy regions are present. These areas are described by conformers A, B, and C, separated by rather small barriers among them. The torsion angle values of ϕ/ψ are: 166.9°/−4.1° for C, 48.9°/0.7° for B, and 63.1°/−150.1° for A. The derived energies account for a nearly equal population distribution around minima B (*syn*, 50%) and A (*anti*, 50%). To evaluate the influence of solvation, the solvent model SM2 was used. After evaluation of the energies, it is observed that the population on B diminishes (Tables 2 and 3), producing a still higher single point population on minimum *anti* A (from 71% to 85%).

Summary of AMBER / Homans, CVFF, and CFF91 calculations. The corresponding calculations already reported [10,11] are summarized in Tables 1–3. The

Table 3
Average $\langle r^{-6} \rangle^{-1/6}$ distances of **2** calculated for the different force fields

Force field	Min	H-1′–H-2′	H-1′–H-3′	H-1′–H-5′	H-1′–H-4	H-1′–H-3	ϕ	ψ	ΔE (kJ/mol)	Single point pop.
AMBER-80	A	3.053	2.574	2.392	3.755	2.081	50	−179.4	13	88.3
	B	3.057	2.585	2.385	2.605	4.687	54.2	22.9	19.81	5.7
	C	3.06	2.58	2.4	3.604	4.777	174.1	4.6	19.72	6.0
AMBER-1* r	A	3.052	2.54	2.509	3.766	2.132	47.6	173.5	116.08	3.5
	B	3.05	2.496	2.491	2.759	4.736	59.7	27.9	145.13	< 0.1
	C	3.058	2.464	2.485	3.605	4.771	−179.8	3.5	107.8	3.5
CFF91-80	A	3.071	2.573	2.385	3.836	2.28	53.6	−176	−210.5	98.0
	B	3.076	2.561	2.363	2.677	4.755	53.1	21.2	−200.26	1.6
	C	3.079	2.564	2.388	3.711	4.788	175.2	3.3	−196.46	0.4
CVFF-80	A	3.091	2.647	2.468	3.848	2.268	50.3	179.4	121.9	90.3
	B	3.092	2.651	2.468	2.674	4.749	53.1	21.5	128.08	7.5
	C	3.093	2.645	2.481	3.713	4.766	172.9	4	131.21	2.2
ESFF-1	A	3.055	2.529	2.527	3.838	2.301	51.4	172.8	271.83	1.0
	B	3.053	2.526	2.501	3.43	4.685	83.1	49.8	286.92	< 0.1
	C	3.072	2.534	2.472	3.671	4.766	−178.4	2.7	260.33	99.0
ESFF-80	A	3.064	2.645	2.367	3.815	2.244	53.5	−177.1	70.89	94.1
	B	3.066	2.645	2.361	2.723	4.744	54.7	24	78.67	4.2
	C	3.068	2.654	2.384	3.688	4.79	173.4	5.1	80.92	1.7
MM3*-1	A	3.111	2.571	2.44	3.842	2.19	44.1	170.6	519.7	41.1
	B	3.111	2.546	2.408	2.618	4.734	52.9	18.4	540	< 0.1
	C	3.114	2.499	2.377	3.704	4.719	−176.5	−2.2	518.8	58.9
MM3*-80	A	3.103	2.617	2.387	3.841	2.135	45.1	177.6	133.9	71.9
	B	3.111	2.62	2.373	2.626	4.732	53.8	18.1	136.5	25.4
	C	3.111	2.599	2.374	3.712	4.763	175.6	1.1	142.1	2.7
MM3*-H_2O	A	3.109	2.578	2.429	3.846	2.199	43.9	170.1	460.4	69.8
	B	3.108	2.581	2.394	2.653	4.734	52.5	21	470.3	1.3
	C	3.113	2.514	2.366	3.71	4.707	−176.5	−2.7	462.6	28.9
AM1	A	3.116	2.666	2.437	3.781	2.098	34.6	172.3	−2101.4	96.1
	B	3.125	2.548	2.399	2.481	4.691	41.2	25.2	−2091.2	1.6
	C	3.123	2.557	2.434	3.64	4.794	172.8	2	−2092.1	2.3

Table 4
Experimental [10] and theoretical population distributions, calculated from the different force fields of the hydroxymethyl groups of **1**

	Population (%)			
	Glc gg	Glc gt	Gal gt	Gal tg
Experimental	60	40	70	30
Force field				
AMBER-80	57	43	65	35
AMBER-1*r	95	5	100	0
CVFF-1	52	48	85	15
CVFF-80	43	57	67	33
CFF91-1	99	1	25	75
CFF91-80	83	17	39	61
MM3*-1	70	30	92	8
MM3*-80	36	64	96	4
MM3-H_2O	90	10	77	23
ESFF-1	10	90	29	71
ESFF-80	45	55	59	41

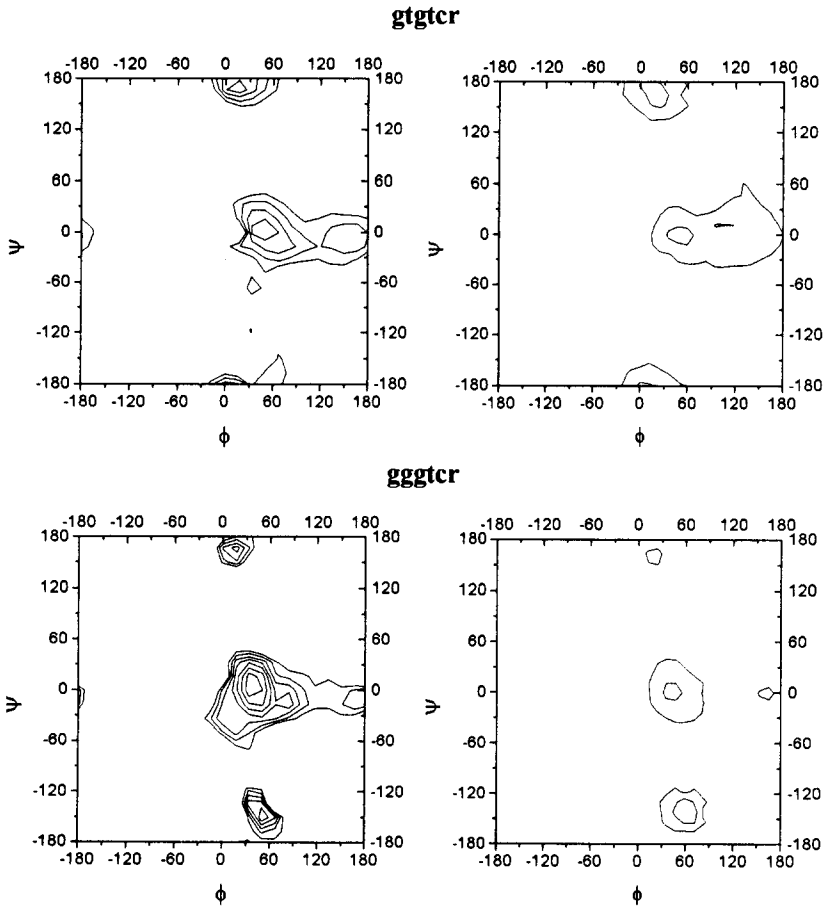

Fig. 4. Steric energy (left) and probability maps (right) determined by AM1 for methyl α-lactoside. The energy levels are represented every 4.18 kJ/mol and the probability levels at 10%, 1%, and 0.1%.

observed results indicate that, for AMBER/Homans, the population distribution of minima A:B:C changes drastically depending on the dielectric constant. Thus, the behaviour is rather similar to that observed for the ESFF force field. At low dielectric constant minimum C is highly populated (> 96%) while at high dielectric constant minimum B is predominant (70%), while A and C show considerable populations, around 15% each. The distribution for the pendant groups is given in Table 4.

For CVFF, the population of region B is greater than 88% (including minimum D) and 96%, for $\varepsilon = 1$ and 80, respectively. The contributions of regions A and C are strongly reduced compared to B and D. The distribution for the pendant groups is given in Table 4.

For CFF91, and $\varepsilon = 1$, most of the population (> 98%) is located around minimum D, thus, in the central *syn* region, but with a geometry which is not favoured by the exo-anomeric effect. With $\varepsilon = 80$, this region is still predominant (59%), but the contribution of minimum B is now higher (36%). The population distribution for the hydroxymethyl groups is also presented in Table 4.

Comparison to NMR data. Fig. 5 shows a representation of the relevant inter-residue proton–proton distances for **1** in terms of the glycosidic torsion angles, superimposed on the probability distribution maps. It can be observed that H-1′/H-3 distance shows intersection with the region corresponding to region A, and therefore the value of the NOE between these two protons will be sensitive to the population around conformer *anti*. In an analogous manner, H-1′/H-4 and H-1′/H-6 NOEs will be representative of the population around conformer B, *syn*. The presence of the H-2′/H-4 NOE will indicate population around region C.

The use of either AMBER or ESFF at low dielectric constant completely fails to reproduce, even qualitatively, the experimental results (Tables 5 and 6 and Fig. 6). On the other hand, the calculations with $\varepsilon = 80$ provide a qualitative agreement: The expected H-1′–H-4 NOE is, in both cases, slightly smaller than the experimental value, thus, the population around conformer *syn* is probably higher than the predicted populations (70% and 79% for AMBER and ESFF, respectively). In turn, the calculated H-1′–H-3 is largely overestimated, indicating that the population of conformer *anti* was overestimated in the calculations (15% and 20% for AMBER and ESFF, respectively). The H-1′–H-6 NOEs are satisfactorily reproduced by both force fields, considering the existence of internal motion around the C-5–C-6 linkage, with a different correlation time to that for the global molecular tumbling. This makes a more quantitative calculation quite difficult. Finally, the population around minimum C is probably around 1–2%, close to that predicted by ESFF-80.

For CVFF, the theoretical H-1′–H-4 NOE values are slightly higher than the experimental ones, especially for $\varepsilon = 80$. On the other hand, the distributions do not reproduce the observed H-1′–H-3 NOE, since they predict very small values for this enhancement. Therefore, the population around region B (*syn* conformer, defined by the H-1′–H-4 NOE) should be smaller than that predicted by CVFF (< 98%). In

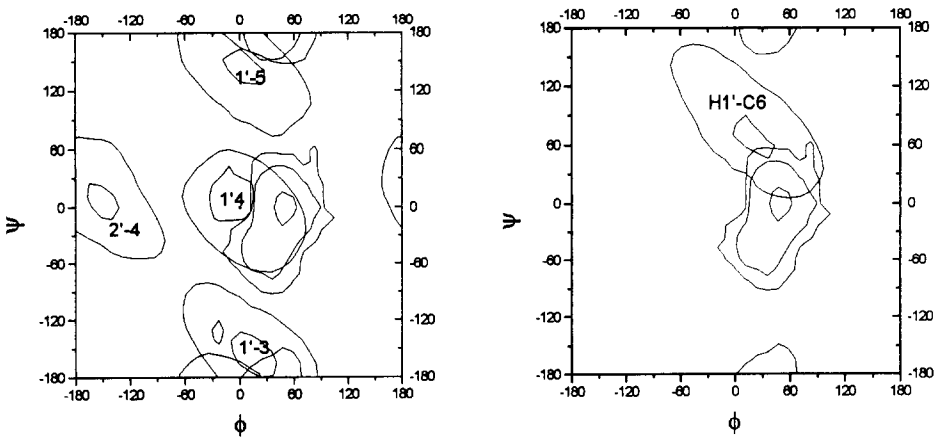

Fig. 5. Superimposition of the key proton–proton short distances on the probability map determined for methyl α-lactoside. Those distances which can provide observable NOEs are indicated.

Table 5
Experimental and estimated (from probability distributions) steady state NOEs of compound **1**

	Intensity (%)											
	Exp. 300 MHz	Exp. 500 MHz	AMBER-80	CVFF-1	CVFF-80	CFF91-1	CFF91-80	ESFF-80	MM3-1	MM3-80	MM3-H_2O	AM1
H-1′–H-2′	7.3	6.5	5.2	6.8	6.8	6.2	6.6	6.6	6.4	6.6	6.5	5.7
H-1′–H-3′	9.8	9.1	8.2	7.1	7.4	8.5	7.7	7.2	8.4	7.6	8.0	8.0
H-1′–H-4′	−2.7	−2.3	−1.9	−1.5	−1.7	−2.1	−2.0	−1.9	−1.8	−1.7	−1.8	−1.5
H-1′–H-5′	10.9	10.0	11.4	8.7	9.1	9.6	10.6	10.9	10.9	11.2	10.8	8.0
H-1′–H-3	4.0	3.5	6.2	0.1	0.1	0.6	1.5	10.0	0.2	1.5	0.0	9.2
H-1′–H-4	13.9	12.7	9.2	13.9	14.8	17.2	15.0	10.7	17.0	15.2	17.8	10.7
H-1′–H-5	–	–	−0.4	0.0	0	−0.3	0	1.0	−0.1	0.0	−0.1	1.9
H-1′–H-6a	1.4	1.0	1.7	0.8	0.8	0	0.7	0.9	0.5	0.8	1.3	1.6
H-1′–H-6b	1.6	1.0	0.6	0.2	1.0	0.0	0	0.8	0.2	1.9	−0.2	0.5

Table 6
Average $\langle r^{-6} \rangle^{-1/6}$ distances of **1** calculated from the sixteen relaxed energy maps for the different force fields. In the case of AM1 only four relaxed energy maps were calculated. The table also contains the calculated experimental NMR distances for **1** and the distances from the X-ray structure of α-lactose (assuming a C–H bond distance of 1.113 Å)

Force field	H-1′–H-2′	H-1′–H-3′	H1′–H-4′	H-1′–H-5′	H-1′–H-3	H-1′–H-4	H-1′–H-5	H-1′–H-6a	H-1′–H-6b	H-2′–H-4
AMBER-80	3.06	2.56	4.02	2.32	2.89	2.52	3.74	2.82	3.09	3.16
CFF91-1	3.05	2.50	4.00	2.45	3.85	2.29	4.49	4.19	5.35	3.95
CFF91-80	3.05	2.50	4.00	2.45	3.56	2.37	4.01	3.21	3.83	4.05
CVFF-1	3.03	2.52	4.01	2.46	4.17	2.38	4.18	3.07	3.47	3.84
CVFF-80	3.03	2.52	4.01	2.46	4.18	2.36	4.13	2.97	3.02	4.15
ESFF-1	3.06	2.59	4.04	2.54	3.63	3.23	4.27	4.06	3.61	2.34
ESFF-80	3.07	2.65	4.07	2.37	2.66	2.50	3.24	2.99	3.06	3.84
MM3*-1	3.12	2.61	4.06	2.40	4.10	2.28	4.21	3.24	3.58	4.18
MM3*-80	3.11	2.65	4.10	2.39	3.58	2.32	3.86	2.90	2.79	4.41
MM3*-H_2O	3.12	2.63	4.09	2.41	4.16	2.28	4.17	3.00	3.83	4.31
AM1	3.15	2.67	4.15	2.54	2.67	2.52	3.06	2.91	3.21	3.78
AM1-SM2	3.15	2.67	4.15	2.53	2.39	2.99	3.78	3.43	5.15	4.41
Exp. NMR	2.9–3.1	2.4–2.6	> 3.5	2.4–2.6	3.1–3.3	2.3–2.5	> 3.5	2.8–3.3	2.8–3.3	> 3.5
X-ray	3.09	2.68	4.13	2.41	4.11	2.07	4.37	3.5	3.66	4.36

addition, the population of the *anti* conformer, A (defined by the H-1′–H-3 NOE), should be more important than that calculated (> 1%). The population of the *gauche–gauche* conformer is probably minor and similar to that deduced by this force field, at $\varepsilon = 80$. The NOEs of the hydroxymethyl groups are reasonably reproduced, especially at $\varepsilon = 80$.

For CFF91, the predicted H-1′–H-4 NOE is largely overestimated, especially at the low dielectric constant. This is the result of the shifting of the population around the central region of the map (conformers *syn*) towards non-exoanomeric values, that is towards region D. In fact, this shifting makes the H-1′–H-6s NOEs unreproducible. On the other hand, the distribution predicts a small H-1′–H-3 NOE at $\varepsilon = 80$. Therefore, the population around region D (*syn* conformer, defined by the H-1′–H-4 NOE) should be smaller than that predicted by CFF91, and the population of *syn* conformers is probably much better defined by region B. In addition, the population of the *anti* conformer, A, should be higher than that calculated (> 2%). The population of the *gauche–gauche* conformer, C, is probably minor and similar to that deduced by this force field, at $\varepsilon = 80$.

For MM3*, the results are almost independent of the conditions employed in the calculations. Nevertheless, the best match between theoretical and observed results is observed for $\varepsilon = 80$. The use of $\varepsilon = 80$ produces a semiquantitative agreement to the observed NOE data: the predicted H-1′–H-4 NOE is slightly overestimated, while the corresponding H-1′–H-3 is clearly underestimated. According to the observed values, the population around region B (*syn* conformer, defined by the H-1′–H-4 NOE) should be smaller than that predicted by MM3* (< 96%). In addition, the population of the *anti* conformer, A, (defined by the H-1′–H-3 NOE) should be slightly higher than that calculated (> 3%). The population of the *gauche–gauche* conformer is probably around 1%, similar to that deduced by this force field, at $\varepsilon = 80$. The NOEs for the Glc hydroxymethyl moiety are correctly reproduced.

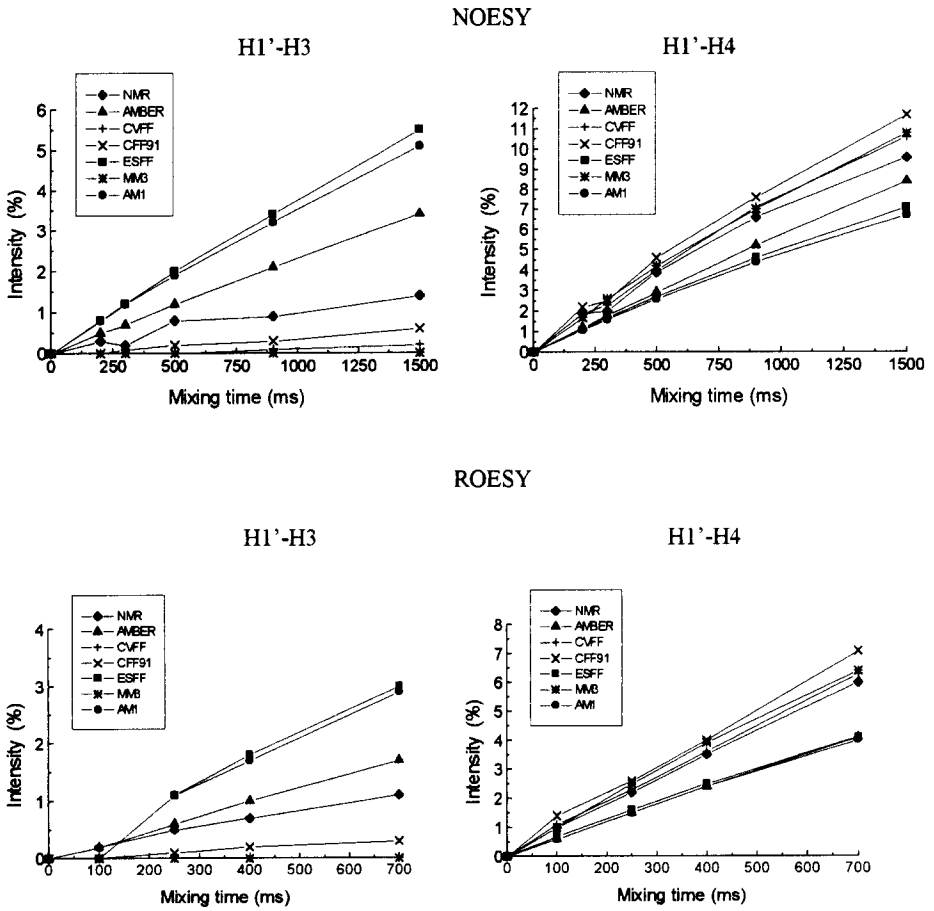

Fig. 6. Experimental and simulated NOESY and ROESY build up curves for the observed interresidue NOEs of methyl α-lactoside.

For AM1, the match between expected and experimental NOEs is poor, since there is an overestimation of the population of the *gauche–gauche* conformer, as also observed in the AMBER/Homans and ESFF calculations. The match is degraded when the SM2 model is used to account for the solvation.

Hydroxymethyl conformations. Gal and Glc H6proR and H6proS were assigned as previously reported for similar derivatives [24]. The distribution of rotamers was calculated following well established methodology [10,24], from the vicinal proton–proton coupling constants, assuming a gg:gt equilibrium for Glc and a gt:tg equilibrium for the Gal rotamers. The observed couplings for the galactose hydroxymethyl group agree satisfactorily with combinations of the gt and tg rotamers, with the gt family most populated (> 65%) [36]. On the other hand the couplings for the glucose lateral chain agree with a ca. 60:40 distribution between the gg and gt conformers. The predicted distributions are gathered in Table 4.

The experimental results are better reproduced when using AMBER/Homans with $\varepsilon = 80$, which gives a complete agreement between observed and predicted data.

The predominance of the gg glucose rotamer and of the gt galactose conformer is also predicted by CVFF ($\varepsilon = 1$), MM3* (GB/SA and $\varepsilon = 1$). Partial agreement is also found with CVFF-80. Finally, the other force fields/dielectric constants predict distributions which strongly deviate from the experimental results.

In conclusion, and after comparison of the different force field and the AM1 calculations with the observed NOE data, it can be deduced that both CVFF and MM3* provide potential energy surfaces that satisfactory agree with the experimental average NOE results. The use of high dielectric constants is recommended in both cases, although the use of the GB/SA model solvent is also advisable in conjunction with MM3*. AMBER and ESFF provide only qualitative agreement with the NMR data and then only at high dielectrics. Regarding the hydroxymethyl lateral chain equilibria, AMBER/Homans, MM3* and CVFF provide distributions that satisfactorily agree with the experimental vicinal coupling constants. CFF91 or AM1 should not be used to perform conformational analysis of disaccharides in solution.

Finally, although the flexibility of methyl α-lactoside in solution is rather limited, regions other than that around the global minimum (conformer *syn*, region B) are also appreciably populated in solution. In particular, the presence of the *anti* A conformer can be deduced from both MM calculations and NOE experiments (H-1′–H-3 NOE).

Molecular mechanics and AM1 results for C-lactose (**2**).—C-lactose (Fig. 1) does not have the interglycosidic oxygen atoms and therefore lacks the possibility of an exo-anomeric effect [37]. To evaluate the importance of this feature in the force field comparison, additional molecular mechanics and semiempirical calculations were performed for **2** using a similar protocol to that described for **1**. Sixteen relaxed energy maps were calculated for **2**, with MM3*, using $\varepsilon = 80$. After calculating the probability distribution (Fig. 7) and the adiabatic map (Fig. 7), three major regions, as also observed for **1**, present energies compatible with their possible existence in equilibrium. The corresponding geometries

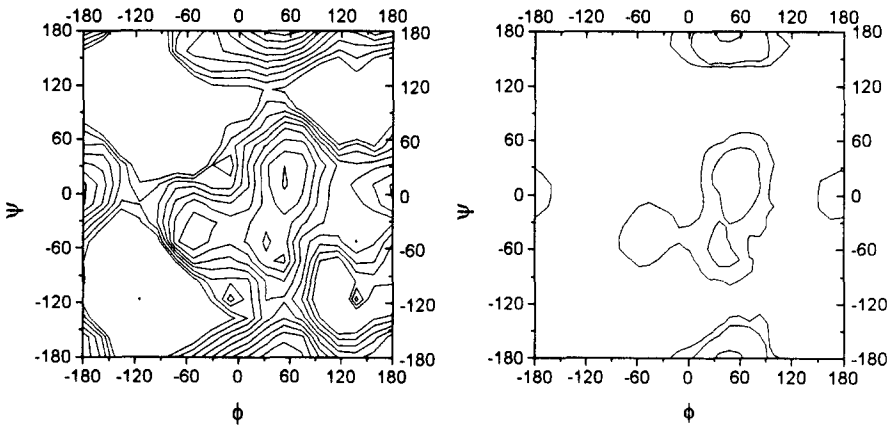

Fig. 7. Steric energy (left) and probability maps (right) determined by MM3* for β-C-lactose using $\varepsilon = 80$. The energy levels are represented every 4.18 kJ/mol and the probability levels at 10%, 1%, and 0.1%.

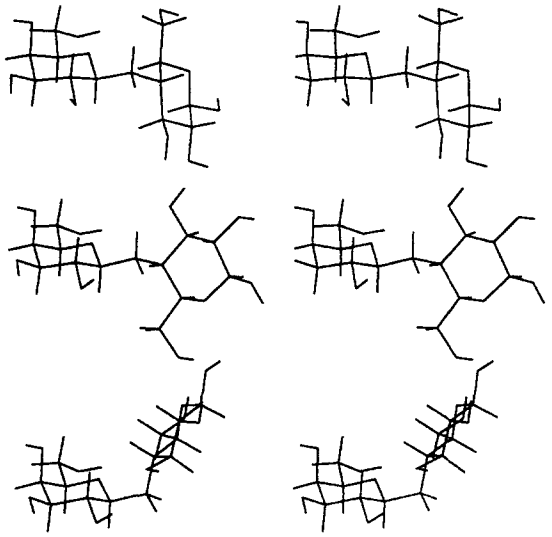

Fig. 8. Stereo view of the major minima of β-C-lactose calculated by MM3*. The interglycosidic torsion angles are fairly similar to those obtained by the different force fields. From top to bottom, conformer *anti*, *syn*, and *gauche–gauche* (see text).

are indeed similar to those deduced for the O-glycoside analogue, **1**, with minor changes around the glycosidic torsion angles. Regarding the shape of the energy and of the distribution maps, it can be observed that the areas which are now populated extend over a broader range of the surfaces, and thus, **2** seems to be much more flexible than its O-glycoside analogue, **1**. In addition, region *anti* (A) and not the central *syn* (B) region now dominates the probability distribution.

The corresponding low-energy geometries (Fig. 8) were also minimized, using the other force fields, producing results which can be grouped into three different cases:

Case 1: For ESFF ($\varepsilon = 1$) and AMBER/Homans ($\varepsilon = r$), minimum C strongly dominates the distribution (> 96%). The contribution of the regions dubbed *anti* and *syn* are basically meaningless.

Case 2: Minimum *anti* is strongly predominant (> 88%). There are minor contributions of regions B (*syn*) and C. This result is observed for AMBER ($\varepsilon = 80$), ESFF ($\varepsilon = 80$), CVFF ($\varepsilon = 80$), CFF91 ($\varepsilon = 80$), and AM1.

Case 3: MM3* results are in between. When using $\varepsilon = 1$ or the GB/SA solvent model, minima A and C are considerably populated, while the contribution of the *syn* region is almost irrelevant. On the other hand, when the calculations are performed with a value of $\varepsilon = 80$, although the *anti* region still dominates the distribution, the population of the *syn* conformer is fairly important (> 25%).

C-lactose (**2**).—*Comparison to NMR results.* The NMR results (NOEs and homonuclear vicinal coupling constants) for a solution of **2** in water have been already described [38] and account for an approximately 50:44:6 equilibrium between regions A:B:C (Fig. 8). A minor contribution of region D to the global population of the *syn* region (mainly described by conformer B) is also possible.

Therefore, and contrary to the experimental observations described for the regular O-glycoside, **1**, the NMR results indicate that, for **2**, the *anti* A conformer is now the major one existing in water solution. This is in sharp contrast to a previous analysis of C-glycoside conformations, which claimed that these synthetic compounds presented similar conformations to their natural analogues [39]. In addition, we have recently reported that the bound [40] conformation of **2** to the galactose-binding protein ricin-B is markedly different to the bound conformation of the natural analogues **1** [36] and **3** [41]. In these two cases, conformers included in the *syn* region, defined by conformers B/D were recognized by the lectin [36]. However, the bound conformation of C-lactose is that corresponding to conformer *anti*, A [40].

The comparison of the molecular mechanics and AM1 calculations to the NMR results allows the following conclusions:

For ESFF, and $\varepsilon = 1$, the results are opposite to the experimental data. On the other hand, the use of $\varepsilon = 80$ predicts that the *anti* conformer dominates the distribution, as observed experimentally. However, the calculated population of B is of only 4%, and, therefore, only a qualitative agreement is found with the NOE data.

The AMBER/Homans results at both dielectric constants are basically identical to those discussed above for ESFF. Both force fields also provided similar results when **1** was used as model compound.

For CVFF and CFF91, and using $\varepsilon = 80$, the same result is again obtained. Therefore, in these four cases, the calculations indicate that the *anti* conformer of C-lactose is more stabilised than the *anti* conformer of **1**, with respect to the corresponding *syn* conformers. Thus, the force field calculations are able to predict, at least qualitatively or semiquantitatively, the experimental observations, which also indicate the predominance of A-region [38]. However, the population of this conformer is overestimated.

For MM3*, the results indicate, in all cases, a destabilization of the *syn* minimum (B) with respect

to the *anti* A conformation. However, and contrary to the results obtained for **1**, the populations of **2** are rather dependent on the dielectric constant employed in the calculations. The best match between theoretical and observed results is observed for $\varepsilon = 80$, which provides an excellent agreement with the observed NOE data, only the population around A is slightly overestimated, while that around B is slightly underestimated, basically in the same proportions. The use of $\varepsilon = 1$ or of the GB/SA solvent model only provides a qualitative agreement, since although the *anti* conformer is the major one predicted in both conditions, the rest of the population is mostly included in region C and not in region B, as observed experimentally.

For AM1, similar results to those found for **1** are observed, since already in the case of the natural O-glycoside, the *anti* A conformer was the major one

Table 7
Bond lengths around the glycosidic linkage calculated by the different force fields for the different minima of compound **1**

Force field	Min	Bond lengths (Å)			
		C-1′–O-5′	C-5′–O-5′	C-1′–O-1′	C-4–O-1′
AMBER-80	A	1.432	1.431	1.399	1.448
	B	1.433	1.433	1.393	1.443
	C	1.431	1.432	1.398	1.452
AMBER-1* r	A	1.427	1.438	1.394	1.445
	B	1.428	1.44	1.391	1.445
	C	1.431	1.44	1.393	1.451
CFF91-80	A	1.434	1.432	1.439	1.444
	B	1.432	1.434	1.434	1.44
	C	1.431	1.434	1.444	1.439
CVFF-80	A	1.457	1.45	1.447	1.434
	B	1.453	1.451	1.432	1.434
	C	1.452	1.451	1.431	1.451
ESFF-1	A	1.425	1.43	1.426	1.431
	B	1.425	1.43	1.423	1.432
	C	1.423	1.429	1.427	1.436
ESFF-80	A	1.427	1.425	1.429	1.43
	B	1.427	1.426	1.424	1.428
	C	1.424	1.425	1.428	1.431
MM3*-1	A	1.419	1.425	1.427	1.433
	B	1.422	1.43	1.426	1.438
	C	1.418	1.425	1.426	1.434
MM3*-80	A	1.425	1.425	1.43	1.435
	B	1.424	1.425	1.424	1.432
	C	1.424	1.425	1.429	1.431
MM3*-H_2O	A	1.424	1.432	1.430	1.437
	B	1.424	1.431	1.427	1.438
	C	1.421	1.431	1.431	1.432
AM1	A	1.416	1.43	1.406	1.434
	B	1.421	1.428	1.414	1.433
	C	1.421	1.429	1.412	1.426
X-ray lactose	B	1.42	1.44	1.39	1.43

in the calculated distribution. The results are now overemphasised, since the population of minimum A is now higher than 96%.

In conclusion, and after comparison of the calculations with the NMR data, it can be deduced that only MM3* (with $\varepsilon = 80$) is able to provide distributions that satisfactorily agree with the experimental average NOE and coupling constant results. The other force fields and the AM1 calculations only provide a qualitative agreement with the NMR data, although indeed they satisfactorily predict which is the major conformer in the distribution.

Table 8
Bond lengths calculated by the different force fields for the minima of the galactose residue of **1**

Force field	Min	Bond lengths (Å)				
		C-1′–C-2′	C-2′–C-3′	C-3′–C-4′	C-4′–C-5′	C-5′–C-6′
AMBER-80	A	1.528	1.529	1.529	1.532	1.529
	B	1.528	1.529	1.529	1.531	1.53
	C	1.532	1.528	1.527	1.532	1.53
AMBER-1*r	A	1.511	1.509	1.52	1.545	1.526
	B	1.513	1.511	1.519	1.546	1.526
	C	1.519	1.508	1.519	1.548	1.529
CFF91-80	A	1.554	1.546	1.544	1.546	1.55
	B	1.551	1.544	1.544	1.545	1.551
	C	1.556	1.546	1.543	1.545	1.551
CVFF-80	A	1.554	1.553	1.558	1.558	1.535
	B	1.553	1.551	1.558	1.56	1.535
	C	1.558	1.552	1.557	1.558	1.535
ESFF-1	A	1.536	1.534	1.539	1.548	1.535
	B	1.535	1.533	1.539	1.551	1.535
	C	1.544	1.533	1.537	1.549	1.535
ESFF-80	A	1.542	1.54	1.541	1.543	1.538
	B	1.54	1.54	1.54	1.544	1.538
	C	1.544	1.539	1.539	1.543	1.538
MM3*-1	A	1.536	1.537	1.538	1.539	1.536
	B	1.541	1.537	1.537	1.537	1.536
	C	1.536	1.537	1.539	1.541	1.538
MM3*-80	A	1.533	1.533	1.531	1.534	1.532
	B	1.535	1.532	1.531	1.534	1.532
	C	1.535	1.532	1.531	1.534	1.532
MM3*-H_2O	A	1.541	1.538	1.538	1.538	1.538
	B	1.543	1.538	1.537	1.537	1.538
AM1	A	1.542	1.536	1.54	1.535	1.533
	B	1.539	1.536	1.54	1.535	1.534
	C	1.539	1.535	1.539	1.535	1.536
X-ray lactose	B	1.531	1.524	1.521	1.517	1.511
Average		1.538	1.535	1.537	1.541	1.535
Min. value		1.511	1.508	1.519	1.517	1.511
Max. value		1.558	1.553	1.558	1.56	1.551
Range		0.047	0.045	0.039	0.043	0.04

Geometry comparison.—Methyl α-lactoside. The structural details of the global and local minima obtained from the molecular mechanics calculations using the five different force fields and the AM1 Hamiltonian are shown in Tables 7–14 along with the details of the crystal structures of α- and β-lactose [12]. The variability of the different structural characteristics of the molecule may have a drastic influence on the derived NMR data which are to be compared to the experimental data. In addition, crystallographic studies allow a direct comparison between observed and modeled structural values.

Table 9
Bond lengths calculated by the different force fields for the minima of the glucose residue of **1**

Force field	Min	Bond lengths (Å)							
		C-1–C-2	C-2–C-3	C-3–C-4	C-4–C-5	C-5–O-5	O-5–C-1	C-1–O-1	C-5–C-6
AMBER-80	A	1.528	1.527	1.533	1.537	1.434	1.433	1.419	1.53
	B	1.53	1.528	1.528	1.533	1.434	1.434	1.418	1.531
	C	1.528	1.527	1.532	1.538	1.435	1.432	1.419	1.532
AMBER-1* r	A	1.526	1.511	1.534	1.539	1.441	1.435	1.419	1.527
	B	1.53	1.509	1.519	1.536	1.44	1.439	1.419	1.526
	C	1.528	1.513	1.521	1.538	1.44	1.437	1.418	1.531
CFF91-80	A	1.546	1.546	1.551	1.561	1.432	1.435	1.434	1.539
	B	1.547	1.546	1.548	1.558	1.433	1.437	1.434	1.538
	C	1.545	1.548	1.55	1.56	1.434	1.435	1.434	1.537
CVFF-80	A	1.553	1.549	1.562	1.568	1.451	1.454	1.441	1.536
	B	1.554	1.549	1.558	1.563	1.452	1.456	1.441	1.536
	C	1.554	1.548	1.562	1.565	1.452	1.454	1.441	1.533
ESFF-1	A	1.537	1.536	1.546	1.55	1.432	1.426	1.43	1.537
	B	1.54	1.533	1.539	1.543	1.432	1.429	1.429	1.537
	C	1.537	1.537	1.542	1.546	1.434	1.425	1.428	1.537
ESFF-80	A	1.54	1.537	1.545	1.55	1.429	1.427	1.428	1.54
	B	1.539	1.538	1.541	1.546	1.428	1.427	1.428	1.539
	C	1.539	1.539	1.542	1.549	1.429	1.428	1.428	1.538
MM3*-1	A	1.54	1.537	1.54	1.535	1.432	1.425	1.425	1.542
	B	1.539	1.533	1.54	1.537	1.432	1.427	1.425	1.537
	C	1.541	1.537	1.537	1.54	1.431	1.425	1.425	1.542
MM3*-80	A	1.532	1.53	1.535	1.535	1.429	1.425	1.426	1.534
	B	1.532	1.529	1.533	1.535	1.428	1.425	1.426	1.533
	C	1.531	1.533	1.537	1.542	1.428	1.424	1.426	1.534
MM3*-H_2O	A	1.542	1.534	1.54	1.536	1.434	1.427	1.426	1.539
	B	1.539	1.535	1.54	1.537	1.432	1.426	1.426	1.538
AM1	A	1.542	1.536	1.534	1.54	1.432	1.41	1.415	1.533
	B	1.541	1.536	1.536	1.537	1.43	1.419	1.411	1.531
	C	1.54	1.536	1.539	1.541	1.431	1.416	1.412	1.531
X-ray lactose	B	1.536	1.523	1.525	1.525	1.435	1.423	1.389	1.502
Average		1.539	1.534	1.54	1.544	1.435	1.431	1.425	1.534
Min		1.526	1.509	1.519	1.525	1.428	1.41	1.389	1.502
Max		1.554	1.549	1.562	1.568	1.452	1.456	1.441	1.542
Range		0.028	0.04	0.043	0.043	0.024	0.046	0.052	0.04

Bond lengths. The bond lengths (Tables 7–9) at the anomeric centers agree best with the crystal structures for the AMBER/Homans force field, which has explicit parameters to deal with the exo-anomeric effect (in this case of a β-glycosidic linkage, shortening of the C-1′–O-1′ distance). In addition, AM1 also provides a satisfactory agreement with the crystal structure. Regarding the rest of the distances along the acetal moiety, all the force fields (and AM1) but CVFF show a satisfactory agreement for C-1′–O-5′ (distance too long 0.03 Å for CVFF). The X-ray C-5′–O-5′ distance is well predicted in all cases. The interglycosidic C-4–O-1′ bond length has a value similar to the other C–O bonds, as predicted by AM1 and other force fields (deviations under 0.01 Å) with the exception of AMBER/Homans, which produces a C-4–O-1′ distance 0.1–0.2 Å higher than the experimental one.

The C–C bonds of the glucose and galactose moieties of **1** are systematically overestimated

Table 10
Bond angles around the glycosidic linkage calculated by the different force fields for the different minima of compound **1**

Force field	Min	Bond angles (°)			
		C-5′–O-5′–C-1′	O-5′–C-1′–O-1′	O-5′–C-1′–C-2′	C-1′–O-1′–C-4
AMBER-80	A	113.7	107.9	110.2	119.8
	B	113.1	107.4	110.1	117.5
	C	113.2	108.3	110	121
AMBER-1* r	A	114.9	107.5	107.7	118.1
	B	113.4	107.5	108.1	116.7
	C	112.8	108.6	108.3	120.1
CFF91-80	A	113.5	109.9	111.9	121.7
	B	113	108.8	111	118.1
	C	112.9	107.8	111	119.1
CVFF-80	A	115.6	112	111.1	119.7
	B	115.4	109.8	110.4	117.4
	C	115.3	109	110.3	120.7
ESFF-1	A	115.9	108.3	111.6	119.3
	B	115.5	107.5	110.5	116.3
	C	116.3	109.7	110.7	120
ESFF-80	A	114.8	110.1	111.9	120.2
	B	114.3	109.3	111	117.3
	C	114.4	109	110.6	120.2
MM3*-1	A	115.2	104.1	108.1	116.2
	B	112.7	106.6	108.2	113.2
	C	114.3	104.9	108.6	118.4
MM3*-80	A	114.2	107.1	109.6	118.9
	B	113.4	108.7	108.1	113.7
	C	113.6	108.3	108	119.9
MM3*-H2O	A	112.8	107.8	109.2	117.5
	B	112.6	106.9	108.8	113.9
	C	112.5	106.6	110.5	118.6
AM1	A	114.1	104.5	111.1	117.6
	B	114	101.8	111.3	114.1
	C	113.6	104	111	118.1
X-ray lactose	B	112.4	107.6	111.4	117.2

Table 11
Bond angles calculated by the different force fields for the minima of the galactose residue of **1**

Force field	Min	Bond angles (°)							
		C-1′–C-2′–C-3′	C-2′–C-3′–C-4′	C-3′–C-4′–C-5′	C-4′–C-5′–C-6′	O-6′–C-6′–C-5′	O-2′–C-2′–C-3′	O-3′–C-3′–C-4′	O-4′–C-4′–C-5′
AMBER-80	A	110.1	110.5	109.5	113	110.3	110.1	110.3	110.3
	B	110.1	110.3	109.6	112.7	110.2	110.1	110.3	110.4
	C	110.2	110.2	109.4	112.6	110.3	109.8	110.3	110.3
AMBER-1* r	A	110	109.2	112.2	112.9	109.4	110.3	110.1	112.1
	B	109.7	109.1	112.3	112.9	109.3	110.2	110.1	112.1
	C	108.8	109	112.6	112.8	109.8	109.5	110.3	112.5
CFF91-80	A	110.1	111.4	109.4	115.7	114.3	109	109.5	108.6
	B	110.5	111.3	109.4	115.6	114.3	109	109.5	108.6
	C	109.6	111.6	109.3	115.6	114.4	108.8	109.3	108.7
CVFF-80	A	110	112	108.9	113.8	111.2	109.9	110	111.1
	B	110.1	112	108.9	113.7	111.2	109.9	110	111
	C	109.9	112	109	113.7	111.2	110	109.9	111.1
ESFF-1	A	111.1	110.8	111	113.1	110.8	109.8	110.7	111.4
	B	110.4	110.5	111.7	113.3	111.5	110.2	110.7	111.6
	C	110.3	110.5	111.5	113.3	111.6	109.8	110.7	111.7
ESFF-80	A	110.9	110.8	110.1	113.5	111.7	110.5	111.2	110.7
	B	110.7	110.7	110.3	113.4	111.8	110.5	111.2	110.8
	C	110.8	110.7	110.2	113.3	111.8	110.5	111.1	110.7
MM3*-1	A	108	110.9	110.2	112.3	110.5	107.4	107.9	109.7
	B	108.5	110.7	109.8	112	110.3	107.2	107.8	109.3
	C	106.9	110.2	110.9	112	110.1	107.7	107.8	109.9
MM3*-80	A	109.7	110.4	109.6	112.3	109.8	106.4	107.8	108
	B	109.7	110.3	109.7	112.4	109.7	107	107.8	107.9
	C	109.6	110.4	109.7	112.3	109.8	106.8	107.8	107.9
MM3*-H_2O	A	108.4	110.1	110.3	111.2	110.9	109.4	107.2	109.3
	B	108.7	110.6	109.6	111.6	110.8	107.2	107.9	109.1
AM1	A	108.9	110.1	109.7	111.7	111	106.8	106.5	108.4
	B	108.7	109.8	109.9	111.7	110.9	107	106.5	108.5
	C	108.7	109.7	110	110.9	110.8	110.4	106.7	108.6
X-ray	B	110.5	110.6	109.4	112.3	110.3	111.3	112	108.9

Table 12
Bond angles calculated by the different force fields for the minima of the glucose residue of **1**

Force field	Min	Bond angles (°)									
		C-1–C-2–C-3	C-2–C-3–C-4	C-3–C-4–C-5	C-4–C-5–C-6	O-5–C-1–C-2	O-6–C-6–C-5	O-2–C-2–C-3	O-3–C-3–C-4	O-1′–C-4–C-5	C-5–O-5–C-1
AMBER-80	A	110.3	109.9	111.1	112.3	109.1	110.4	110.2	110.1	111.2	114.8
	B	110.5	109.8	110.4	112.7	109.4	110.9	110.3	110.2	110	115
	C	110.4	110.1	109.3	114	109.3	111	110.3	110.7	110	115.1
AMBER-1* r	A	108.3	110.6	108.7	111.7	108.7	109.5	107.6	113.1	109.9	115.7
	B	108.8	109.4	109.1	111.4	108	109.4	107.1	111.5	111.6	115.1
	C	109.3	109.9	108	113.4	109.2	110.3	107.6	113.3	110.7	115.6
CFF91-80	A	111.8	110.1	113.5	113.4	110.5	114.3	114.1	108.3	112.9	114.3
	B	111.8	110.3	111.7	113.8	110.7	114.3	114.3	108.9	109.4	114.2
	C	112	110.2	110.8	114.6	110.7	114.1	114.3	109.5	108.7	114.1
CVFF-80	A	110.7	111.4	110.7	111.7	109.7	110.1	110.2	109.4	114.5	116.7
	B	110.7	111.6	109.4	112	109.9	110.1	110.3	109.5	110	116.3
	C	110.8	111.6	108.6	112.7	109.9	110.2	110.4	109.9	110.5	116.4
ESFF-1	A	110.9	110.9	111.6	112.9	110.2	110.8	110.9	111.8	112.1	114.6
	B	111	110.4	111.9	112.9	109.6	111.7	111.2	110.2	110.3	113.8
	C	111.2	111	110.3	113.6	110.3	110.8	111	112.1	110.2	114.9
ESFF-80	A	111	110.3	112.1	112.8	110.3	111.8	111.4	110.8	113.9	115.8
	B	111.5	110.2	110.6	113	110.6	111.9	111.4	111.3	110.3	115.5
	C	111.5	110.4	110	113.7	110.5	112	111.5	111.5	110.2	115.5

MM3*-1	A	111	108.4	109.3	112.6	110	109.8	108.7	108.9	111.8	114.5
	B	110.4	108.4	109.2	111.8	108.8	111.3	110	110.3	107.1	113.6
	C	111.7	108	107.3	113.7	110.2	113.2	108.3	111.3	105.7	114.1
MM3*-80	A	111.2	108.2	110.9	111.9	108.5	109.7	109.4	108.4	111.3	114.8
	B	111.4	108.6	109.8	112.1	108.5	109.8	109.4	108.7	107.7	114.8
	C	112	108.4	107.8	112.4	108.6	109.8	109.8	109.4	105	114.4
MM3*-H_2O	A	109.6	107.9	110.8	112.2	109.4	111.7	110.3	109.1	112.2	114.8
	B	110.6	108.8	109.3	111.9	109	111.7	110.1	110.1	106.8	114
AM1	A	109	108.9	110.4	110.9	112.5	112.1	112.1	111.9	109.2	115.5
	B	109.9	108.7	110.3	111.3	111.4	112.1	112.2	111.4	107.7	114.8
	C	109.4	108.7	109	112.4	111.1	112.9	112.1	111.7	107	115.2
X-ray	B	110.7	110.7	110.8	113.3	109.7	110.8	113	111.4	106.8	114.3
Average		110.6	109.7	110.1	112.6	109.8	111.3	110.7	110.5	109.8	114.9
Min.		108.3	107.9	107.3	110.9	108	109.4	107.1	108.3	105	113.6
Max.		112	111.6	113.5	114.6	112.5	114.3	114.3	113.3	114.5	116.7
Range		3.7	3.7	6.2	3.7	4.5	4.9	7.2	5	9.5	3.1

by CFF91 and CVFF, with lengths more than 0.02 Å larger than the crystal structure, while the rest of force fields show differences under this limit. In addition, all the force fields studied herein clearly overestimate the C-5–C-6 distance for both Glc and Gal residues of **1**, the difference being around 0.03 Å.

Values of the H–H distances may have a drastic impact on the derived NOE intensities [14]. In fact, it is common to employ the so called isolated spin pair approximation (ISPA) for the experimental determination of unknown interproton distances based on NOE measurements [14]. In this protocol, a standard distance for a known intraresidue proton pair is taken as reference along with its corresponding NOE cross peak volume measured in a NOESY experiment carried out with a short mixing time. On this basis, variations in the reference distance may lead to considerable errors when calculating unknown distances for proton pairs located in different moieties of the

Table 13
Torsion angles calculated by the different force fields for the minima of the galactose residue of **1**

Force field	Min	Torsion angles (°)					
		C-1′–C-2′–C-3′–C-4′	C-2′–C-3′–C-4′–C-5′	C-3′–C-4′–C-5′–O-5′	C-4′–C-5′–O-5′–C-1′	C-5′–O-5′–C-1′–C-2′	O-5′–C-1′–C-2′–C-3′
AMBER-80	A	−53.2	54	−57.4	62.6	−61.7	55.6
	B	−53.5	54.3	−57.4	62.1	−61.3	55.8
	C	−53.8	55	−57.5	61.5	−60.2	55
AMBER-1*r	A	−57.3	49.3	−48.3	55.8	−63.4	64
	B	−58	49.6	−47.6	55	−63.1	64.2
	C	−60.4	49.8	−44.4	51.3	−61.8	65.6
CFF91-80	A	−50.2	52	−57.2	63.3	−61.4	53.6
	B	−50.1	51.9	−57.2	63	−60.8	53.3
	C	−50.4	53.3	−57.5	62	−59.6	52.3
CVFF-80	A	−52.6	53.5	−55.4	60.8	−59.4	53
	B	−52.5	53.5	−55.3	60.6	−59.1	52.8
	C	−52.6	54.4	−55.7	59.5	−57.5	51.8
ESFF-1	A	−52.5	50.4	−50.6	55.6	−57.1	54.3
	B	−53.9	49.2	−48.1	53.9	−58.5	57.5
	C	−53.5	50.7	−49.2	52.7	−55.8	55.3
ESFF-80	A	−50.7	51.7	−55.7	61.4	−60.1	53.4
	B	−51	51.8	−55.3	60.5	−59.7	53.7
	C	−50.6	52.9	−56	59.3	−57.3	51.7
MM3*-1	A	−55	52.3	−53.3	62.1	−65.8	59.6
	C	−58.4	52.5	−49.6	57.8	−65.2	62.8
	B	−54.3	52.6	−55.5	64.6	−66.8	59.6
MM3*-80	A	−53.1	54.9	−58	63.6	−62.5	55
	B	−53.6	53.5	−57.2	65.3	−65.4	57.4
	C	−53.6	53.5	−57.1	65.4	−65.5	57.4
MM3*-H_2O	A	−53.7	53.6	−56.1	62.1	−63.9	58.3
	B	−53.9	53.2	−56.5	64.6	−65.9	58.6
AM1	A	−55.3	53.1	−53.3	57.6	−59.7	57.9
	B	−56.1	53.6	−52.6	56	−58.7	58.1
	C	−56.7	53	−51.3	55	−58.5	58.9
X-ray lactose	B	−51.1	54.5	−59.3	63.2	−60	53.2
Average		−53.7	52.6	−54.2	59.9	−61.2	56.7
Min.		−60.4	49.2	−59.3	51.3	−66.8	51.7
Max.		−50.1	55	−44.4	65.4	−55.8	65.6
Range		10.3	5.8	14.9	14.1	11	13.9

glycosidic linkages. Indeed, deviations in the H-1′–H-3′ and H-1′–H-5′ reference distances of up to 0.26 and 0.24 Å are found, respectively. In addition, and although the position of the hydrogens in X-ray data is only approximated, it can be observed that the best agreement between modeled and experimental data is found when MM3* is used, independent of the dielectric constant. This fact also underlines the importance of the election of the force field whenever a model capable of reproducing the experimental data is needed.

Bond angles. The anomeric O-5′–C-1′–O-1′ bond angle presents a value of around 107.6° in the crystal structure of α-lactose. All force fields basically agree with this value, with the exception of the CVFF and AM1 calculations which overestimate and underestimate the value, respectively (Tables 10–12). In the case of the MM3* results, it can be observed that the bond angle value is affected by the dielectric constant. Indeed, at low dielectrics, where electrostatic interactions are more important, the higher deviations are found. A similar value is found with AM1, where

Table 14
Torsion angles calculated by the different force fields for the minima of the glucose residue of **1**

Force field	Min	Torsion angles (°)					
		C-1–C-2–C-3–C-4	C-2–C-3–C-4–C-5	C-3–C-4–C-5–O-5	C-4–C-5–O-5–C-1	C-5–O-5–C-1–C-2	O-5–C-1–C-2–C-3
AMBER-80	A	−54.5	52.6	−53.4	59.3	−61.5	57.5
	B	−54.9	54.3	−55.1	59.4	−59.7	56
	C	−55.6	54.9	−55.5	59.8	−59.5	55.9
AMBER-1*r	A	−60.3	56.2	−52	56.4	−59.7	59.6
	B	−60.8	57.6	−54.4	57.9	−60.1	59.9
	C	−59.6	59.1	−56.6	58.3	−57.6	56.4
CFF91-80	A	−49	45.8	−49.3	57.4	−61.3	56.3
	B	−49.5	48.9	−53.2	59.4	−60	54.2
	C	−49.9	49.9	−54.6	60.5	−59.8	53.6
CVFF-80	A	−53.2	51.2	−51	57	−58.7	54.7
	B	−53.4	53.2	−53.9	58.7	−57.8	53.1
	C	−53.7	54	−54.7	59.4	−57.7	52.8
ESFF-1	A	−50.9	48.5	−51	58.7	−61.3	56.1
	B	−51.6	48.2	−50.9	58.7	−61.7	57.5
	C	−51.3	50.7	−53.6	59.8	−59.7	54.2
ESFF-80	A	−51.8	49.5	−50.5	56.8	−59.5	55.6
	B	−51.6	51.9	−54.3	58.8	−58.1	53.2
	C	−51.9	52.4	−55	59.3	−57.9	52.9
MM3*-1	A	−54.6	56.6	−59.1	61.5	−58.7	54.6
	B	−56.9	55.1	−56.6	60.9	−60.9	58.6
	C	−55.3	58.9	−62.5	62.8	−56.7	52.7
MM3*-80	A	−55	54.2	−56.1	61	−61.4	57.4
	B	−54.9	54.9	−57.4	62.1	−60.7	56.2
	C	−55.2	56.9	−60.8	64.2	−59.6	54.4
MM3*-H_2O	A	−57.4	55.8	−55.1	58.2	−60.1	58.9
	B	−56.1	54.6	−56.2	60.7	−60.4	57.7
AM1	A	−56.3	56.1	−53.7	53.8	−55.2	55.7
	B	−54.8	55.9	−56.4	57.9	−57.6	55.2
	C	−57.2	57.4	−56.2	57.1	−56.8	55.9
X-ray lactose	B	−51	53.3	−57.1	63.1	−61.7	53.8
Average		−54.3	53.6	−54.9	59.3	−59.4	55.7
Min.		−60.8	45.8	−62.5	53.8	−61.7	52.7
Max.		−49	59.1	−49.3	64.2	−55.2	59.9
Range		11.8	13.3	13.2	10.4	6.5	7.2

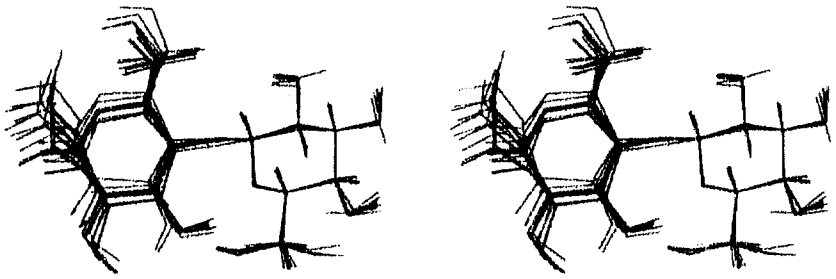

Fig. 9. Superimposition of the different *syn* minima found for the different force fields for methyl α-lactoside.

a reduction of the charge on O-1′ with respect to O-5′ is deduced. This reduction probably lowers the repulsion energy between these two oxygens, thus affecting the bond angle value.

The ring oxygen angle (C-5′–O-5′–C-1′) of α-lactose in the solid state presents a value of 112.4° (113.3° for β-lactose). The values provided by CVFF and ESFF for **1** are remarkably higher, while those

Table 15
Bond distances around the glycosidic linkage calculated by the different force fields for the minima of compound **2**

Force field	Min	Bond lengths (Å)			
		C-1′–O-5′	C-5′–O-5′	C-1′–C-α	C-4–C-α
AMBER-80	A	1.436	1.435	1.544	1.552
	B	1.438	1.437	1.54	1.552
	C	1.437	1.436	1.541	1.556
AMBER-1* r	A	1.435	1.44	1.544	1.555
	B	1.438	1.445	1.543	1.555
	C	1.437	1.446	1.538	1.556
CFF91-80	A	1.43	1.433	1.548	1.559
	B	1.433	1.433	1.545	1.558
	C	1.431	1.434	1.55	1.562
CVFF-80	A	1.448	1.445	1.541	1.548
	B	1.452	1.449	1.544	1.555
	C	1.452	1.447	1.543	1.553
ESFF-1	A	1.425	1.427	1.544	1.555
	B	1.426	1.432	1.546	1.557
	C	1.426	1.433	1.541	1.553
ESFF-80	A	1.426	1.426	1.546	1.553
	B	1.428	1.426	1.544	1.554
	C	1.426	1.425	1.546	1.556
MM3*-1	A	1.425	1.428	1.54	1.554
	B	1.425	1.43	1.537	1.561
	C	1.426	1.433	1.537	1.562
MM3*-80	A	1.426	1.426	1.54	1.551
	B	1.426	1.425	1.536	1.559
	C	1.425	1.426	1.538	1.564
MM3*-H_2O	A	1.426	1.429	1.541	1.555
	B	1.427	1.43	1.538	1.56
	C	1.427	1.433	1.538	1.563
AM1	A	1.429	1.427	1.527	1.519
	B	1.43	1.428	1.526	1.522
	C	1.43	1.429	1.525	1.523

provided by AMBER, CFF91, and MM3* are fairly similar to the experimental observations. AM1 values are slightly high.

The glycosidic bond angle C-1′–O-1′–C-4 of crystalline α-lactose presents a value of 117.2° (116.5° for β-lactose, **3**), in agreement with other reported observations for β-glycosidic linkages. The conformation around the glycosidic linkage strongly influences this value, and, independent of the force field used in the calculations, the smallest values of this bond angle are found for minimum B, while the highest values are encountered for C conformers. Minima within region A show intermediate values. The comparison of the calculated bond angles for all B minima with that of the crystal (also in region B of the map), shows that only MM3* and AM1 underestimate the value (ca. 3°).

Pyranose conformation. Both pyranoid rings, independently of the starting structure, remained during the minimization protocol in the $^4C_1$ chair conformations.

In general, the pyranoid torsion angles deduced by the calculations are fairly similar (Tables 13 and 14) for the galactose and glucose moieties of **1**. Thus, only those for the non-reducing galactose moiety will be discussed. Generally, the torsion angle values depend on the force field used, on the dielectric constant, and on the region of the map in which the corresponding conformer is found. In particular, the best agreements with the crystal structure of **1** are

Table 16
Bond distances calculated by different force fields for the galactopyranoid rings of the different energy minima of **2**

Force field	Min	Bond lengths (Å)				
		C-1′–C-2′	C-2′–C-3′	C-3′–C-4′	C-4′–C-5′	C-6′–O-6′
AMBER-80	A	1.54	1.536	1.535	1.538	1.535
	B	1.54	1.536	1.534	1.537	1.535
	C	1.543	1.536	1.534	1.536	1.535
AMBER-1* r	A	1.539	1.534	1.534	1.543	1.535
	B	1.538	1.532	1.533	1.544	1.534
	C	1.54	1.529	1.534	1.547	1.533
CFF91-80	A	1.56	1.549	1.544	1.543	1.538
	B	1.557	1.548	1.544	1.543	1.538
	C	1.561	1.547	1.544	1.542	1.538
CVFF-80	A	1.561	1.553	1.555	1.555	1.534
	B	1.558	1.552	1.554	1.556	1.534
	C	1.557	1.552	1.554	1.556	1.535
ESFF-1	A	1.543	1.539	1.538	1.548	1.537
	B	1.542	1.535	1.537	1.546	1.535
	C	1.546	1.532	1.537	1.547	1.535
ESFF-80	A	1.547	1.541	1.539	1.543	1.538
	B	1.547	1.54	1.539	1.542	1.539
	C	1.548	1.539	1.538	1.542	1.538
MM3*-1	A	1.54	1.538	1.535	1.537	1.538
	B	1.538	1.537	1.536	1.537	1.535
	C	1.539	1.534	1.537	1.539	1.536
MM3*-80	A	1.538	1.532	1.531	1.534	1.533
	B	1.536	1.532	1.531	1.534	1.532
	C	1.537	1.531	1.531	1.534	1.533
MM3*-H_2O	A	1.541	1.539	1.538	1.538	1.539
	B	1.54	1.538	1.537	1.538	1.537
	C	1.54	1.536	1.538	1.539	1.537
AM1	A	1.538	1.539	1.537	1.533	1.533
	B	1.538	1.539	1.535	1.535	1.533
	C	1.537	1.537	1.538	1.535	1.533

found when CFF91, CVFF, and ESFF calculations are performed at high dielectric constants, as well as when AMBER ($\varepsilon = 1^*r$) is used. High deviations are found with AMBER-80. MM3* and AM1 values are in between. Nevertheless, MM3* with $\varepsilon = 80$ provide angles closer to the experimental results than when used with $\varepsilon = 1$ or with the GB/SA solvent model. Fig. 9 shows a superimposition of the different B (*syn*) minima of the galactose pyranoid ring with the corresponding X-ray structure. The shape of the chairs is fairly similar in all cases.

C-lactose.—Bond lengths. Due to the lack of anomeric effects in compound **2**, the C1′–O5′ and C5′–O5′ are basically similar, independently of the force field used in the calculations, including the AM1 results. In addition, C-1′–O-5′ is remarkably similar for compounds **1** and **2** with differences smaller than 0.01 Å (Tables 15–17). The major differences are found for the AMBER-1*r and the AM1 calculations.

The interglycosidic distance C-1′–C-α is found to be shorter (around 0.01 Å) than the C-4–C-α one in the majority of the calculations. The only exceptions are found when AM1 is used, for which C-1′–C-α is found to be larger by 0.02–0.08 Å than the C-4–C-α. The major differences are found when the MM3* force field is used. In this case, differences up to around 0.026 Å are encountered.

Regarding the C–C ring bond lengths of the glucose and galactose moieties of **2**, it is observed that,

Table 17
Bond distances calculated by different force fields for the glucopyranoid rings of the different low energy minima of **2**

Force field	Min	Bond lengths (Å)							
		C-1–C-2	C-2–C-3	C-3–C-4	C-4–C-5	C-5–O-5	O-5–C-1	C-1–O-1	C-5–C-6
AMBER-80	A	1.532	1.53	1.542	1.55	1.442	1.432	1.425	1.538
	B	1.531	1.53	1.54	1.55	1.44	1.43	1.426	1.538
	C	1.53	1.528	1.54	1.552	1.441	1.431	1.425	1.54
AMBER-1*r	A	1.529	1.526	1.54	1.554	1.445	1.428	1.42	1.54
	B	1.53	1.528	1.541	1.552	1.445	1.428	1.42	1.538
	C	1.53	1.525	1.537	1.55	1.447	1.428	1.42	1.54
CFF91-80	A	1.545	1.545	1.562	1.556	1.434	1.428	1.425	1.538
	B	1.546	1.544	1.556	1.555	1.434	1.428	1.425	1.538
	C	1.545	1.544	1.559	1.557	1.434	1.426	1.425	1.539
CVFF-80	A	1.545	1.55	1.567	1.561	1.451	1.441	1.421	1.535
	B	1.544	1.548	1.569	1.567	1.451	1.439	1.422	1.535
	C	1.545	1.547	1.567	1.568	1.45	1.438	1.422	1.537
ESFF-1	A	1.532	1.533	1.545	1.556	1.43	1.416	1.404	1.538
	B	1.53	1.531	1.55	1.561	1.432	1.414	1.404	1.539
	C	1.532	1.532	1.543	1.553	1.431	1.415	1.404	1.539
ESFF-80	A	1.537	1.538	1.548	1.555	1.427	1.422	1.415	1.54
	B	1.537	1.538	1.547	1.556	1.427	1.421	1.414	1.54
	C	1.536	1.537	1.547	1.556	1.427	1.421	1.415	1.54
MM3*-1	A	1.537	1.535	1.539	1.541	1.43	1.42	1.417	1.542
	B	1.537	1.535	1.537	1.542	1.429	1.42	1.418	1.538
	C	1.537	1.534	1.538	1.542	1.431	1.42	1.417	1.54
MM3*-80	A	1.53	1.532	1.539	1.54	1.426	1.422	1.419	1.534
	B	1.53	1.532	1.538	1.542	1.426	1.422	1.419	1.532
	C	1.53	1.531	1.539	1.543	1.426	1.422	1.419	1.533
MM3*-H_2O	A	1.539	1.538	1.54	1.541	1.429	1.42	1.418	1.543
	B	1.539	1.538	1.539	1.542	1.429	1.42	1.418	1.539
	C	1.539	1.537	1.539	1.541	1.429	1.42	1.418	1.541
AM1	A	1.541	1.537	1.534	1.529	1.434	1.418	1.401	1.534
	B	1.539	1.537	1.534	1.531	1.432	1.42	1.401	1.533
	C	1.541	1.536	1.534	1.532	1.433	1.417	1.401	1.535

as observed for **1**, those provided by the CFF91 and CVFF force fields are about 0.02 Å longer than those calculated by the other energy functions.

Finally, with respect to the C-5–C-6 distances of the hydroxymethyl moieties of **2**, it is found that they show basically the same values as those found for **1**, that is distances around 0.03 Å longer than those found in the crystal structure of **1**.

From a global comparison, and when considering all the low energy geometries provided by the different programs, it is found that the maximum differences for a given proton–proton intraresidue distances can reach up to 0.16 Å, that is, significantly smaller than those found for **1**. In addition, for a given force field, there are also clear variations of the proton–proton intraresidue distances of **1** compared to those of **2**. These can amount up to 0.13 Å.

Bond angles. The bond angle O-5′–C-1′–C-α of **2** present a range of values between 105.5° and 109.7°, depending on the force field. In general, there is no dependence on the dielectric constant, although the values depend on the minimum which is considered (Tables 18–20). The smallest values are found for CFF91, MM3*, and AM1, while the largest angles are provided by AMBER, CVFF, and ESFF.

The interglycosidic C-1′–C-α–C-4 bond angle has a considerably lower value than its analogue of **1**, independent of the force field. This is probably due to the higher distances between the two sugar units of **2** with respect to **1**. Thus, the C-linkage reduces the

Table 18
Bond angles around the glycosidic linkage calculated by the different force fields for the minima of compound **2**

Force field	Minimum	Bond angles (°)			
		C-5′–O-5′–C-1′	O-5′–C-1′–C-α	O-5′–C-1′–C-2′	C-1′–C-α–C-4
AMBER-80	A	115.7	109.7	109.5	113.8
	B	115.4	109.1	109.9	111.6
	C	115.7	109.6	110.3	112.3
AMBER-1* r	A	117.2	108	109.1	113.3
	B	116.5	109	109.2	112.4
	C	116	109.5	109.4	112.3
CFF91-80	A	113.7	107.3	110.4	118.2
	B	113.2	106.5	110.5	115
	C	113.8	107.5	111	116.5
CVFF-80	A	116	109.3	109.7	118.6
	B	115.7	108.6	110.2	114
	C	116	109.7	110.8	116.2
ESFF-1	A	117.3	108	109.3	117.4
	B	116.3	109.2	110.1	119.4
	C	115.5	109	110.7	116
ESFF-80	A	115.1	109.7	110.2	118.2
	B	114.9	108.7	110.5	115.6
	C	115.3	109.2	111.2	116.7
MM3*-1	A	115.2	105.8	107.8	116.3
	B	114	106.3	108.1	113.7
	C	113.1	107.4	108.2	115.5
MM3*-80	A	113.9	107.7	108	117.3
	B	113.6	106.5	108.2	113.7
	C	113.8	107.4	108.7	115.9
MM3*-H_2O	A	114.8	106.3	108	116.6
	B	113.5	106.7	108.7	114.2
	C	113	107.4	108.5	115.8
AM1	A	113.9	105.5	110.3	115
	B	113.1	105.9	108.9	112.3
	C	113.4	107	109.9	113.7

Table 19
Bond angles calculated by different force fields for the galactopyranoid rings of the different energy minima of **2**

Force field	Min	Bond angles (°)							
		C-1′–C-2′–C-3′	C-2′–C-3′–C-4′	C-3′–C-4′–C-5′	C-4′–C-5′–C-6′	O-6′–C-6′–C-5′	O-2′–C-2′–C-3′	O-3′–C-3′–C-4′	O-4′–C-4′–C-5′
AMBER-80	A	110.7	110.9	109.6	113.2	110.7	109.7	110.5	110.5
	B	110.7	110.9	109.5	113.1	110.6	109.7	110.4	110.5
	C	110.6	110.7	109.6	113.1	110.7	109.8	110.4	110.5
AMBER-1*r	A	110.3	111.6	111.1	112.4	110.9	108.6	110.1	111.6
	B	109.9	110.9	111.4	112	110.2	109	110.1	111.6
	C	109.6	110.2	111.7	111.9	110.3	110	110.2	111.4
CFF91-80	A	110.1	110.9	109.4	114.6	114.1	113	109.7	108.8
	B	109.9	111.1	109.6	114.5	114	109.5	109.5	108.7
	C	109.8	111.1	109.5	114.5	114.1	109.3	109.4	108.7
CVFF-80	A	110	112.4	108.8	113.1	109.9	109	109.9	111.2
	B	110.1	112.3	108.8	112.9	110	109.1	109.9	111.1
	C	110	112.2	108.8	112.8	110	109.3	109.9	111.2
ESFF-1	A	110.2	110.3	111	112.7	111.5	110.5	110.2	111.6
	B	110.5	110.5	111.1	112.3	110.5	109.2	110.7	111.4
	C	110.3	110.1	111.1	112.2	110.5	109.9	110.7	111.4
ESFF-80	A	111.2	110.8	110	113.3	111.8	110.2	111.1	110.8
	B	111.1	110.9	110	113.3	111.8	110	111.2	110.9
	C	111.2	110.8	110	113.2	111.8	109.9	111.1	110.8
MM3*-1	A	108.8	110.8	109.9	111.5	110.9	106.7	107.8	109.8
	B	108.6	110.3	110	111.7	110.1	107.3	107.8	109.9
	C	108.3	109.6	110.4	111.3	110.5	108.2	107.9	109.6
MM3*-80	A	109.9	110.2	109.8	111.9	110	107.6	107.6	107.9
	B	109.7	110.3	109.7	112.4	109.7	106.9	107.8	107.9
	C	109.6	110.1	109.7	112.2	109.9	107	107.8	107.9
MM3*-H_2O	A	109	110.6	109.9	111.4	111.3	107.4	107.7	109.4
	B	109.1	110.3	109.9	111.5	110.8	108.1	107.6	109.5
	C	108.6	109.7	110.1	111.3	110.9	108.4	107.9	109.2
AM1	A	110.6	110.8	108.9	111.6	110.8	104.7	106.6	108.6
	B	109.2	110	109.5	111.4	110.9	105.4	106.7	108.6
	C	109.3	109.8	109.6	111.1	111.1	106.2	106.7	108.5

Table 20
Bond angles calculated by different force fields for the glucopyranoid rings of the different energy minima of **2**

Force field	Min	Bond angles (°)							
		C-1–C-2–C-3	C-2–C-3–C-4	C-3–C-4–C-5	C-4–C-5–C-6	O-6–C-6–C-5	O-2–C-2–C-3	O-3–C-3–C-4	C-α–C-4–C-5
AMBER-80	A	110.2	110.6	109.4	114.1	110.7	110.2	110.7	115.6
	B	110.6	111	109.6	114	110.9	110.2	110.4	113
	C	110.1	111.3	110.3	113.8	110.9	110.2	110.4	113.3
AMBER-1* r	A	109.3	111.1	109.5	114.8	109.9	110.1	110.6	115.5
	B	109.9	111.1	108.7	114.6	110.6	110.2	110.8	114
	C	109.2	111	110.6	113.1	110.5	110.1	110.8	113.6
CFF91-80	A	111	111.9	109.7	115.1	113.9	109	109.1	116.8
	B	111.2	112.2	110.2	115.1	114.2	108.9	108.5	113.2
	C	110.9	112.4	109.9	115.1	114.1	108.9	108.8	113.5
CVFF-80	A	110.1	112.1	109.3	114	110	109.8	110.6	116.2
	B	110.1	112.4	108.6	114.2	110.2	109.8	110.1	113.2
	C	109.9	112.5	109	113.5	110.2	109.9	110.2	113
ESFF-1	A	111	111.6	110.1	114.8	110.1	110.6	110.7	115.8
	B	110.5	111.8	109.1	116.4	110.5	110.6	111.4	117.2
	C	110.5	111.3	110.5	113.5	110.5	110.4	111	114.6
ESFF-80	A	110.6	111.1	110	114.1	112	110.7	111.2	115.6
	B	110.7	111.6	109.7	114.5	112.1	110.7	110.9	113.5
	C	110.5	111.7	110	114.2	112.1	110.7	111.1	113.5
MM3*-1	A	108.3	110.4	109	113.4	110	107.7	108.2	114.1
	B	108.6	110.5	108.7	113.1	110.4	107.7	108	111.9
	C	108	110	109	112.5	110.4	107.5	109.1	112.2
MM3*-80	A	109.9	110.1	109.2	113.1	109.6	107.1	108.2	114.2
	B	110.1	110.3	108.8	113.3	109.7	107.1	107.9	112.1
	C	109.9	110.3	108.6	113.2	109.7	107.1	108.3	112.1
MM3*-H_2O	A	108.6	111	109.2	113.5	110.2	107.6	107.8	113.9
	B	108.9	110.9	108.5	113.5	110.8	107.6	107.8	112
	C	108.3	110.5	108.9	112.8	110.7	107.5	108.4	112.2
AM1	A	109.6	109.8	109.8	112.1	111	106.7	107.5	112.9
	B	110.4	109.8	108.1	113.2	111.1	106.5	107.9	111.7
	C	109.5	110	109.4	111.5	111	106.7	107.7	111.4

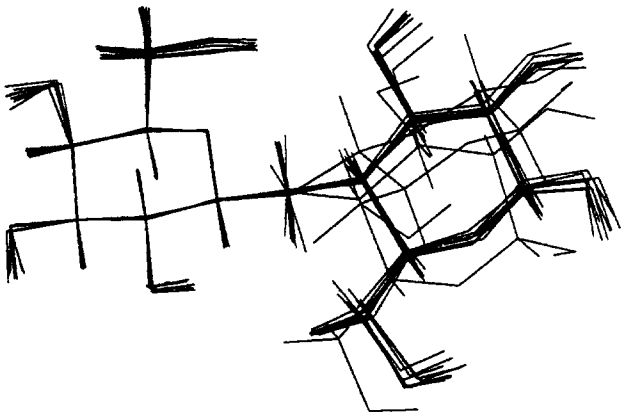

Fig. 10. Superimposition of the different *syn* minima found for the different force fields for β-C-lactose. MM3* *anti* and *gauche–gauche* are also superimposed.

interunit steric effects without opening the corresponding glycosidic bond angle. A conformational dependence of this bond angle, similar to that previously mentioned for **1**, is also observed in **2**. Thus, minimum B always presents the lowest values, while minima C and A present the intermediate and highest value, respectively. The range of values offered by the different force fields oscillate between 111.6° and 115.6°, with AMBER and AM1 presenting the smallest values and CFF91 and ESFF showing the greatest ones.

Pyranoid conformations. There are no remarkable differences among the galactose and glucose pyranoid rings. The major differences are found when all the obtained are compared directly (Tables 21 and

Table 21
Torsion angles calculated by different force fields for the different energy minima of **2**

Force field	Min	Torsion angles (°)					
		C-1′–C-2′–C-3′–C-4′	C-2′–C-3′–C-4′–C-5′	C-3′–C-4′–C-5′–O-5′	C-4′–C-5′–O-5′–C-1′	C-5′–O-5′–C-1′–C-2′	O-5′–C-1′–C-2′–C-3′
AMBER-80	A	−53.2	54.1	−55.9	60.8	−59.2	53.4
	B	−53	54.4	−56.4	60.7	−58.7	53
	C	−53.2	55	−56.5	59.8	−57.7	52.6
AMBER-1*r	A	−54	50.8	−49.5	55.9	−58.8	55.5
	B	−55.6	51.1	−48.8	54.5	−58.7	57.5
	C	−56.8	51.9	−48.7	53.7	−58.8	58.9
CFF91-80	A	−51.3	53.1	−57.5	63.1	−61	53.7
	B	−51.1	52.5	−57	63.1	−61.6	54.3
	C	−51.1	53.3	−57.2	62.2	−60.1	53.1
CVFF-80	A	−52.3	53.5	−55.4	61.5	−59.6	52.3
	B	−52.3	53.7	−55.6	60.9	−58.9	52.2
	C	−52.4	54.3	−55.6	59.8	−57.5	51.5
ESFF-1	A	−55.3	51.4	−49.4	54.8	−58.1	56.6
	B	−54.5	50.9	−49.6	54.4	−57.4	56.2
	C	−54.6	51.6	−50.4	54.3	−57.1	56.4
ESFF-80	A	−50.8	52	−55.7	61.2	−59.3	52.5
	B	−50.7	52.1	−55.9	61	−59	52.5
	C	−50.4	52.8	−56.1	60	−57.3	51.1
MM3*-1	A	−55.4	53	−53.7	62.1	−64.4	58.4
	B	−56	52.6	−53.4	61.5	−64.7	60
	C	−57	52.9	−53.2	60.7	−65.1	61.9
MM3*-80	A	−54	53.8	−57	64.6	−64.6	57.2
	B	−53.8	53.7	−57.2	64.9	−64.9	57.2
	C	−54.1	54.3	−57.3	64	−63.9	56.9
MM3*-H_2O	A	−55	53.2	−54.5	62.6	−64.4	58.2
	B	−54.6	53.1	−55.3	62.6	−64.2	58.5
	C	−56.2	53.3	−54.5	61.7	−64.9	60.7
AM1	A	−52.8	52.6	−55.8	60.7	−59	54.4
	B	−56.4	52.3	−53.3	59.6	−62.1	60
	C	−56.4	53	−53.2	57.9	−60.1	58.9

Table 22
Torsion angles calculated by different force fields for the different energy minima of **2**

Force field	Min	Torsion angles (°)					
		C-1–C-2–C-3–C-4	C-2–C-3–C-4–C-5	C-3–C-4–C-5–O-5	C-4–C-5–O-5–C-1	C-5–O-5–C-1–C-2	O-5–C-1–C-2–C-3
AMBER-80	A	−52.7	52.6	−56.7	62.9	−63	57
	B	−51.7	51.2	−56.1	63.2	−63.2	56.6
	C	−52.1	50.1	−53.7	61.6	−63.7	57.9
AMBER-1*r	A	−53.9	52.4	−54.7	61	−63	58.2
	B	−52.9	53	−56.9	63	−62.7	56.6
	C	−53.6	51.1	−52.8	59.7	−63.3	59.1
CFF91-80	A	−47.5	49	−56.4	65.7	−64	53.4
	B	−47	47.5	−54.9	64.7	−63.9	53.6
	C	−47.6	47.7	−54.4	64.3	−63.8	53.9
CVFF-80	A	−52.8	51.9	−53	60.3	−60.7	54.5
	B	−52.7	51.8	−53.2	60.7	−60.7	54.3
	C	−53.1	51.5	−52	59.6	−60.6	54.8
ESFF-1	A	−49.7	49.5	−53.3	59.9	−60	53.6
	B	−51.4	51.7	−53.8	59.8	−59.4	53.2
	C	−51.3	50.6	−52.4	58	−59.1	54.2
ESFF-80	A	−50.9	50.9	−54.3	60.6	−60.6	54.2
	B	−50.5	50.2	−54	61.1	−60.9	54
	C	−50.8	49.6	−52.6	60	−60.9	54.7
MM3*-1	A	−54.9	54.6	−57.3	64.7	−65.7	58.8
	B	−54	54.8	−58.6	65.8	−65.7	57.8
	C	−55.9	55.7	−57.6	64.1	−65.3	59.1
MM3*-80	A	−53.6	53.8	−58	66	−65.6	57.4
	B	−53.2	53.9	−58.8	66.8	−65.6	56.8
	C	−54	54.2	−58.2	66.3	−65.5	57.2
MM3*-H_2O	A	−53.1	53.5	−57.4	65.6	−66	57.5
	B	−52.8	54.6	−59.4	67	−65.8	56.5
	C	−54.5	55.3	−58.1	65.1	−65.3	57.7
AM1	A	−54.3	54	−55.4	59.3	−59.5	56.4
	B	−54.3	55.8	−58.4	61.3	−58.2	54.2
	C	−55	54.3	−55.2	58.9	−59.1	56.4

22). In fact, ESFF and MM3 ($\varepsilon = 80$) provide the largest variation for the C-4–C-5–O-5–C-1 torsion angle (10°) of the galactose moiety. The observed values are even more similar for the glucose ring. A superimposition of the different minima is presented in Fig. 10.

4. Conclusions

In conclusion, the force field comparison presented herein indicates that the use of the MM3* and CVFF force fields provide conformer distributions of **1** which satisfactorily account for the experimental solution NMR data [10]. Therefore, as found for the regular MM3 or for the CHARMm force fields [35], they are appropriate for use in conformational analysis of carbohydrates. Other force fields such as AMBER/Homans, ESFF, and CFF91 only provide qualitative agreement with the experimental data. On the other hand, it is shown that the semiempirical AM1 method does not correctly reproduce the population distribution of **1** in water solution, even with the addition of the SM2-AMSOL model. From a geometric point of view, the agreement between the structural characteristics of the different minima and the experimental solid state data for methyl α-lactoside, **1**, indicates that the basic shape of the pyranoid ring does not drastically change among the different force fields although minor structural details are affected.

In particular, only AMBER and AM1 provide good bond lengths near the anomeric center. With respect to C-lactose, it is again shown that MM3* provides a population which accounts for the experimental NMR data [38]. The other force fields and the AM1 method only provide qualitative agreements between the modeled and observed data.

Acknowledgements

Financial support by DGICYT (grant PB93-0127) is gratefully acknowledged. The authors are grateful to Prof. M. Martín-Lomas for his interest and support throughout this work and to Prof. R.R. Schmidt and to Dr. H. Dietrich for providing a sample of compound **2**.

References

[1] (a) K.G. Rice, P. Wu, L. Brand, and Y.C. Lee, *Curr. Opin. Struct. Biol.*, 3 (1993) 669–674; (b) R.J. Woods, *Curr. Opin. Struct. Biol.*, 5 (1995) 591–598.

[2] (a) K. Gessler, N. Krauss, T. Steiner, C. Betzel, C. Sandmann, and W. Saenger, *Science*, 266 (1994) 1027–1029; (b) T. Steiner and W. Saenger, *Carbohydr. Res.*, 259 (1994) 1–12.

[3] (a) C.A. Bush, *Curr. Opin. Struct. Biol.*, 2 (1992) 655–660; (b) M. Hricovini, R.N. Shah, and J.P. Carver, *Biochemistry*, 31 (1992) 10018–10023; (c) P.J. Hajduk, D.A. Horita, and L. Lerner, *J. Am. Chem. Soc.*, 115 (1993) 9196–9201; (d) S.W. Homans, *Glycobiology*, 3 (1993) 551–555.

[4] (a) Lommerse et al., *J. Biomol. NMR*, 5 (1995) 79–94. H. van Halbeek, *Curr. Opin. Struct. Biol.*, 4 (1994) 697–709; (b) S. Perez, *Curr. Opin. Struct. Biol.*, 3 (1993) 675–680; (c) F. Mohamadi, N.G.J. Richards, W.C. Guida, R. Liskamp, C. Caufield, G. Chang, T. Hendrickson, and W.C. Still, *J. Comput. Chem.*, 11 (1990) 440–467.

[5] A.D. French and J.W. Brady (Eds.), *Computer Modeling Carbohyds. Molecules ACS*, 430 (1990).

[6] T.M. Glennon, Y.J. Zheng, S.M. Le Grand Bashutzberg, and K.M. Merz Jr., *J. Comput. Chem.*, 15 (1994) 1019–1040.

[7] M.K. Dowd, A.D. French, and P.J. Reilly, *J. Carbohydr. Chem.*, 14 (1995) 589–600.

[8] R.U. Lemieux and S. Koto, *Tetrahedron*, 30 (1974) 1933–1944.

[9] (a) A.J. Kirby, *The Anomeric Effect and Related Stereoelectronic Effects at Oxygen*, Springer, New York, 1983; (b) I. Tvaroska and T. Bleha, *Adv. Carbohydr. Chem. Biochem.*, 47 (1989) 45–123.

[10] J.L. Asensio and J. Jiménez-Barbero, *Biopolymers*, 35 (1995) 55–73.

[11] (a) J.L. Asensio, M. Martín-Pastor, and J. Jiménez-Barbero, *Int. J. Biol. Macromol.*, 17 (1995) 137–148; (b) J.L. Asensio, M. Martín-Pastor, and J. Jiménez-Barbero, *J. Mol. Struct. THEOCHEM*, in press.

[12] K. Hirotsu and A. Shamada, *Bull. Chem. Soc. Jpn.*, 47 (1974) 1872–1879.

[13] (a) D.A. Cumming and J.P. Carver, *Biochemistry*, 26 (1987) 6664–6676; (b) J.P. Carver, S.W. Michnick, A. Imberty, and D.A. Cumming, *Carbohydrate Recognition in Cellular Function*, Wiley, New York, 1989, CIBA Foundation Symp. 145, pp 6–26; (c) J.P. Carver, *Pure Appl. Chem.*, 65 (1993) 763–770.

[14] D. Neuhaus and M.P. Williamson, *The Nuclear Overhauser Effect in Structural and Conformational Analysis*, VCH Publishers, New York, 1989.

[15] M. Eberstadt, G. Gemmecker, D.F. Mierke, and H. Kessler, *Angewandte Chem. Int. Ed. Engl.*, 34 (1995) 1671–1695.

[16] S. Perez, A. Imberty, and J.P. Carver, *Adv. Comp. Biol.*, 1 (1994) 147–202.

[17] J.F. Espinosa, M. Martín-Pastor, J.L. Asensio, H. Dietrich, M. Martín-Lomas, R.R. Schmidt, and J. Jiménez-Barbero, *Tetrahedron. Lett.*, 35 (1995) 6329–6332.

[18] S.W. Homans, *Biochemistry*, 29 (1990) 9110–9118.

[19] A.T. Hagler, P. Lifson, and P. Dauber, *J. Am. Chem. Soc.*, 101 (1979) 5122–5130.

[20] J. Maple, U. Dinur, and A.T. Hagler, *Prot. Nat. Acad. Sci. USA*, 85 (1988) 5350–5354.

[21] N.L. Allinger, Y.H. Yuh, and J.H. Lii, *J. Am. Chem. Soc*, 111 (1989) 8551–8559.

[22] *Extensible Systematic Force Field*, Biosym Technol. Inc., San Diego, USA, 1994.

[23] F. Mohamadi, N.G.J. Richards, W.C. Guida, R. Liskamp, C. Caufield, G. Chang, T. Hendrickson, and W.C. Still, *J. Comput. Chem.*, 11 (1990) 440–467.

[24] K. Bock and J.O. Duus, *J. Carbohydr. Chem.*, 13 (1994) 513–543.

[25] W.C. Still, A. Tempczyk, R.C. Hawley, and T. Hendrickson, *J. Am. Chem. Soc.*, 112 (1990) 6127–6129.

[26] M.J.S. Dewar, E.G. Zoebisch, E.F. Haly, and J.J.P. Steward, *J. Am. Chem. Soc.*, 107 (1985) 3902–3909.

[27] M.J.S. Dewar and W. Tiuel, *J. Am. Chem. Soc.*, 99 (1977) 4899–4906.

[28] M. Khahl, R.J. Woods, D.F. Weaver, and V.H. Smith Jr., *J. Comput. Chem.*, 12 (1991) 584–593.

[29] C.J. Cramer and D.G. Truhlar, *Science*, 256 (1992) 213–219.

[30] J.H. Noggle and R.E. Schirmer, *The Nuclear Overhauser Effect: Chemical Applications*, Academic, New York, 1971, pp 90–93,

[31] P. Cagas and C.A. Bush, *Biopolymers*, 30 (1990) 1123–1138.

[32] M. Bernabé, A. Fernández-Mayoralas, J. Jiménez-Barbero, M. Martín-Lomas, and A. Rivera, *J. Chem. Soc., Perkin Trans. 2.*, (1989) 1867–1873.

[33] (a) Y. Bourne, P. Rouge, and C. Cambilleau, *J. Biol. Chem.*, 267 (1992) 197–203; (b) A. Imberty, Y. Bourne, C. Cambilleau, P. Rouge, and S. Perez, *Adv. Biophys. Chem.*, 3 (1993) 71–118.

[34] M.K. Dowd, A.D. French, and P.J. Reilly, *Carbohydr. Res.*, 233 (1992) 15–36.

[35] S.B. Engelsen, S. Perez, I. Bracani, and C. Herve du Penhoat, *J. Comput. Chem.*, 16 (1995) 1096–1119.
[36] J.L. Asensio, F.J. Cañada, and J. Jiménez-Barbero, *Eur. J. Biochem.*, 233 (1995) 618–630.
[37] K. Bock and S. Refn, *Acta Chem. Scand., Sect. B*, 41 (1987) 469–472.
[38] K.N. Houk, J.E. Ekstrowicz, Y.D. Wu, C.D. Fuglevang, and D.B. Mitchell, *J. Am. Chem. Soc*, 115 (1993) 4170–4177.
[39] A. Wei, A. Handrechy, C. Audin, J. Hyuk-Sang, N. Handrechy-Bretel, and Y. Kishi, *J. Org. Chem.*, 57 (1992) 482–489.
[40] J.F. Espinosa, F.J. Cañada, J.L. Asensio, H. Dietrich, R.R. Schmidt, and J. Jiménez-Barbero, *Angewandte Chem. Int. Ed. Engl.*, 35 (1996) 303–306.
[41] V.L. Bevilacqua, D.S. Thomson, and J.H. Prestegard, *Biochemistry*, 29 (1990) 5529–5537.